https://doi.org/10.5194/egusphere-2026-5460
Preprint. Discussion started: 21 September 2026

On the Range of Marine Cloud Brightening Radiative Forcing across Earth System Models

Haruki Hirasawa[1], Knut von Salzen[1], Matthew Henry[2], Josh Smith[2], Frida A.-M. Bender[3], Cindy Wang[4], Sarah Doherty[1], Robert Wood[1], Philip J. Rasch[1], and James Haywood[2]

[1]Department of Atmospheric and Climate Science, University of Washington, Seattle, WA, USA
[2]Department of Mathematics, University of Exeter, UK
[3]Department of Meteorology and Bolin Centre for Climate Research, Stockholm University, Stockholm, Sweden
[4]Department of Earth and Atmospheric Sciences, Cornell University, Ithaca, NY, USA

Correspondence: Haruki Hirasawa (harukih@uw.edu)

Abstract. Marine cloud brightening (MCB) is a solar radiation modification method that involves using injections of sea salt aerosol (iSSA) particles to increase cloud albedo and cool surface climate. Earth system models (ESMs) are crucial tools for projecting the potential climate response to MCB, but they must represent many key aerosol and cloud processes using parameterizations that are often poorly constrained and can vary substantially. Here, we conduct simulations in six ESMs, plus four alternate modified parameterizations versions, to compute effective radiative forcing (ERF) from MCB iSSA emissions in three subtropical regions. We a find large range in ERF across the nine models with appropriate aerosol activation, with iSSA mass emissions to get -2 Wm^{-2} ranging from 7 Tg yr^{-1} to 93 Tg yr^{-1}in models. The emitted iSSA size distribution drives much of this spread, as the ESMs use median modal radii ranging from 28.1nm to 72.5nm, resulting in major differences in CCN concentration. Forcing from aerosol-cloud interactions drives the majority of the total ERF below about -2 Wm^{-2} across seven of ten models. At high emission rates, the aerosol-cloud forcing saturates, but the direct aerosol forcing continues to increase sufficiently quickly such that there is no regime in which additional appropriately-sized iSSA emissions would cause warming in any of the ESMs. After accounting for iSSA size distribution, the spread in aerosol-cloud interaction forcing is mainly due to differences in cloud adjustments at low emission rates and mainly due to cloud droplet activation saturation at high emission rates.

1 Introduction

Marine cloud brightening (MCB) is a proposed solar radiation modification climate intervention in which sea salt aerosol injections (iSSA) would be used to increase the atmospheric albedo and cool surface temperatures, with the aim of offsetting some impacts of global warming (Latham et al., 2008; Feingold et al., 2024). Research on the potential feasibility, benefits, and harms of MCB deployment must resolve uncertainties across a range of scales requiring an array of modeling, observational, and experimental approaches (Diamond et al., 2022; Feingold et al., 2024; Doherty et al., 2026). Many key physical science questions can be addressed through high resolution modeling and outdoor studies. However, to assess the potential climate impacts of MCB we must rely heavily on Earth system models (ESMs), as MCB tests large enough to measurably perturb

https://doi.org/10.5194/egusphere-2026-5460
Preprint. Discussion started: 21 September 2026

temperatures would essentially be deployments (Doherty et al., 2026). Thus, continued assessment and improvement of ESMs are essential to enabling credible assessments of MCB potential feasibility, benefits, and harms.

The amount of cooling from MCB is primarily driven by the effective radiative forcing (ERF) generated by the iSSA emissions. The ERF from iSSA injection is due to atmospheric albedo changes from 1) iSSA acting as cloud condensation nuclei (CCN), activating into cloud droplets, and influencing sunlight reflection by clouds (aerosol cloud interaction - ACI, ERF_{aci}) and 2) direct sunlight scattering by the aerosols themselves (aerosol radiation interaction - ARI, ERF_{ari}). These processes are critical to MCB representation, since the MCB ERF is the main driver of inter-model differences in MCB response, whereas the pattern of climate response to a given forcing is comparatively robust across ESMs (Rasch et al., 2024; Hirasawa et al., 2026a). They also together represent the largest source of uncertainty in characterizing the total anthropogenic forcing (Bellouin et al., 2020), owing to the difficulty in treating a range of aerosol processes including aerosol emissions, formation, and deposition, and cloud processes including cloud droplet activation, aerosol-induced precipitation suppression, entrainment enhancement, and the turbulence and dynamical organization of clouds. Some processes that are generically important to aerosol anthropogenic forcing are less relevant for MCB specifically, such as cloud adjustments to atmospheric warming by absorbing aerosol, secondary organic aerosol precursor emissions and particle formation, and aerosol mixing states. However, the concentrated marine aerosol perturbations that are associated with MCB amplify the importance of other processes, like aerosol coagulation, cloud droplet activation, and enhancement of dry air entrainment. In the following subsections, we discuss some of the key processes for MCB and their representation in ESMs.

1.0.1 Aerosol Radiation Interactions

The strength of the aerosol radiation interaction ERF_{ari} from iSSA emissions (A.K.A. marine sky brightening (MSB)) depends on the representation of aerosols in ESMs. Past ESM studies have suggested that the ERF from iSSA emissions intended for MCB is predominantly due to the ERF_{ari} effect (Ahlm et al., 2017; Mahfouz et al., 2023; Haywood et al., 2023), meaning ERF_{ari} representation is crucial for the overall efficacy of iSSA emissions. Aerosol size distribution influences ERF_{ari}, as Mie scattering calculations indicate that sea salt aerosol particles tend to be most efficient per mass at reflecting sunlight at dry radii of ∼0.2-0.3μm, which is larger than the sizes typically targeted when MCB iSSA are optimized to be CCN, i.e. 0.03-0.05μm (Connolly et al., 2014; Wood, 2021). Thus, the contribution of MSB relative to MCB will be overestimated if the injected iSSA emissions are larger than is optimal for MCB. Furthermore, many ESMs use modal aerosol representations that are designed for computational efficiency and to represent aerosol distributions commonly observed today. Those modal treatments are not necessarily configured to accurately represent the iSSA size distribution with mean and variance values that would match the distribution expected for MCB or MSB. Because natural SSA are predominantly larger coarse mode particles, many models have limited representation of the smaller Aitken and accumulation mode sea salt aerosol particles that are important for accurately representing MCB and MSB. These practical limitations make it difficult to use consistent iSSA size distributions across ESMs (Rasch et al. (2024); Table 1), which has downstream effects on MCB ERF, including on the per-particle scattering by the iSSA and thus ERF_{ari}.

https://doi.org/10.5194/egusphere-2026-5460
Preprint. Discussion started: 21 September 2026

ERF_{ari} per emitted iSSA mass will be greater in ESMs with longer tropospheric iSSA atmospheric lifetimes. Aerosol lifetimes are sensitive to the aerosol wet and dry deposition rates, and proximity of the aerosols to precipitation and the surface. Aerosols that are mixed higher into the troposphere thus tend to have longer lifetimes (Kristiansen et al., 2016). Dry deposition is driven by Brownian diffusion for small particles and sedimentation, turbulent transport, and surface properties for large particles (Petroff and Zhang, 2010). Wet deposition is driven by the parameterization of in-cloud and below-cloud scavenging efficiency of aerosols by precipitation (Dana and Hales, 1976; Jones et al., 2022), which is a significant source of inter-ESM spread due to differences in deep convection, precipitation formation, and aerosol hygroscopicity representations. Together these processes result in troposphere aerosol lifetimes for sulphate-like particles ranging from a few days to a few weeks (Kristiansen et al., 2016). Considering iSSA have similar properties to sulphate aerosol, iSSA lifetime uncertainties may be similarly large.

ERF_{ari} also depends on underlying and adjacent cloud cover (Ghan, 2013) and underlying surface reflectance (Derimian et al., 2016) below scattering aerosols, with underlying high albedo surfaces being associated with weaker or even positive ERF_{ari}. The underlying surface albedo over oceans is relatively consistent across ESMs. Therefore, we might expect that the modeled climatological low cloud cover is more important for determining the ERF_{ari} strength over marine regions (Vignesh et al., 2020). In the subtropical regions we focus on here, differences in shallow convection, cloud microphysics, and radiation parameterizations contribute the inter-model spread in low cloud cover, which will modulate the strength of ERF_{ari}.

1.0.2 Aerosol Cloud Interactions

Model differences in MCB ERF_{aci} depend on the representation of a range of aerosol and cloud processes. These are typically categorized into the cloud albedo effect (Twomey or first indirect effect) and cloud adjustments which modulate the cloud albedo effect (e.g., the Albrecht or second indirect effect, plus any modulations to cloud cover induced by aerosol). Both the albedo effect and cloud adjustments are driven by iSSA acting as effective CCN, activating as they rise into clouds to become cloud droplets. Increasing cloud droplet number concentration (N_d) with constant cloud liquid water content results in smaller cloud droplets, which in turn increases shortwave scattering by the droplets (thus increasing cloud albedo); in response to having smaller droplets, precipitation formation is reduced and cloud-top entrainment and droplet evaporation are altered (thus driving cloud adjustments).

Aerosol activation into cloud droplets is relatively well understood but can differ substantially between models depending on the specifics of how aerosol size and composition are represented, the aerosol activation parameterization, and the vertical velocity used to drive drop activation (which in turn often depends upon the planetary boundary layer turbulence parameterization used in a given model). Following κ-Köhler theory, the activation rate depends on the relative humidity, vertical velocity, number of aerosol particles, aerosol size distribution, and aerosol hygroscopicity. In the context of MCB, this means the size distribution and emission rate of the iSSA particles play leading roles in determining the resulting activation rate and thus ERF_{aci} from MCB iSSA emissions.

ESM simulations with a popular activation parameterization proposed by Abdul-Razzak and Ghan (2000) (hereafter ARG2000) suggest that accumulation mode iSSA (dry radii ~100nm) are most efficient in terms of albedo change per mass of emissions

https://doi.org/10.5194/egusphere-2026-5460
Preprint. Discussion started: 21 September 2026

(Alterskjaer and Kristjánsson, 2013; Haywood et al., 2023; Rasch et al., 2024). This is because, with this activation scheme, the injection of particles smaller than this results in vapour competition, so the particles do not have access to enough water vapour to grow into cloud droplets. For particles larger than this, the mass of iSSA increases rapidly with radius and substantially faster than the rate at which the activation rate increases. However, more detailed modeling using parcel models that explicitly calculate activation suggest that the vapour competition behaviour for smaller aerosol sizes is unrealistically strong in ARG2000, since the scheme does not account for kinetic limitations in CCN water uptake, resulting in excessively strong activation suppression (Phinney et al., 2003; Connolly et al., 2014; Ghosh et al., 2025; Riipinen et al., 2026). As noted above, these more detailed models indicate that smaller iSSA with dry radii ∼15-30 nm are the most efficient per mass to enhance N_d and increase cloud albedo (Connolly et al., 2014; Wood, 2021).

ESMs also differ substantially in how they parameterize the vertical velocity distribution used to compute droplet activation. These are typically determined by planetary boundary layer turbulence parameterizations which tend to be a significant source of spread among ESMs (Holtslag et al., 2013; Virtanen et al., 2025). The activation rate also decreases as background N_d increases, resulting in reduced MCB effectiveness when there are more natural and anthropogenic aerosol emission sources in the MCB perturbation regions (Carslaw et al., 2013; Hirasawa et al., 2026a). In addition to aerosol activation, the cloud albedo effect depends on factors such as background low cloud fraction, cloud and aerosol concentrations above the clouds being brightened, and background cloud optical thickness.

The cloud adjustment effect refers to changes in the macroscopic properties of clouds due to increased N_d and the resulting radiative forcing. The first set of processes is driven by the suppression of precipitation formation in warm liquid clouds by N_d increases. As cloud droplet radii decrease, the rate at which they grow into rain droplets (undergo autoconversion) also decreases (Albrecht, 1989). This reduces the rate at which water is removed from the clouds, increasing their liquid water content and thus their optical thickness. It also inhibits the breakup of stratiform clouds, resulting in longer cloud lifetimes and the time-averaged cloud fraction in certain regions (Chen et al., 2022; Yuan et al., 2023). Both effects enhance the SW cloud forcing from MCB. However, reduced droplet sizes also tend to increase dry air entrainment into the clouds, which reduces cloud thickness and water content, reducing cloud albedo. This entrainment enhancement arises from reduced precipitation evaporation below the clouds as precipitation is suppressed (Wood, 2007), reduced sedimentation rate as droplets get smaller (Bretherton et al., 2007), and an increased evaporation rate (or "deactivation") of cloud droplets as they get smaller (Karset et al., 2020). As a result of these competing cloud thickening and thinning processes, the net effect of cloud adjustments to aerosols is highly uncertain. ESMs tend to represent only a subset of the relevant processes driving these responses. While many modern ESMs consider the dependence of cloud droplet autoconversion on droplet concentration, few represent the full effect of N_d on entrainment (Karset et al., 2020). Thus, ESMs may overestimate the extent to which cloud adjustments enhance the initial Twomey forcing (Bender et al., 2019; Mülmenstädt et al., 2024).

An additional set of processes arises from aerosol interactions with deep convective clouds. Different theories have been proposed which suggest that increased aerosol concentrations could increase the strength of convection within clouds involving solely liquid phase as well as mixed phase processes (Varble et al., 2023). Observations of the relevant processes are sparse, thus the strength of these effects is poorly constrained. Nevertheless, if MCB aerosol indeed invigorated convection, we would

https://doi.org/10.5194/egusphere-2026-5460
Preprint. Discussion started: 21 September 2026

expect decreased outgoing longwave radiation from higher cloud tops and increased shortwave reflection from increased cloud optical thickness (Lohmann, 2017; Nishant et al., 2019). The coupling between deep convection and cloud microphysics parameterizations tend to be limited in ESMs with convective parameterizations themselves varying substantially and the relevant processes depending on both ice and liquid microphysics. Thus, we do not assess the aerosol effect on deep convective clouds in this study and focus on marine boundary layer low clouds.

1.0.3 Study outline

Together, the issues above with accurately representing MCB (and, aerosol-cloud interactions more generally) mean that ESMs produce a wide range of forcings for a given aerosol perturbation. As such, they cannot be relied on to accurately quantify MCB efficacy at global scales. Nonetheless, they are the scientific community's most important tool for estimating the potential impacts of MCB interventions. A clear understanding of model structural and parametric uncertainty is needed to inform assessments of MCB efficacy. Here, we seek to expand on the initial work of Rasch et al. (2024) (hereafter R2024) to: (1) quantify the range in MCB ERF for a given iSSA injection rate across a larger set of models, (2) identify the key processes driving inter-model differences, and (3) propose steps for enabling more credible estimates of MCB efficacy in future ESM simulations. We present an inter-comparison of the ERF from subtropical MCB iSSA emissions in six CMIP6-generation ESMs and four additional cases with modified microphysical parameterizations. This is the largest model intercomparison of MCB iSSA forcing to date, enabling a broader examination of the aerosol and cloud processes underlying the atmospheric response to MCB than previous work. In section 2, we describe the models, simulation protocol, and analysis methods used in this work. In section 3, we compare the total (ERF_{tot}), aerosol-cloud (ERF_{aci}), and aerosol-radiation (ERF_{ari}) forcing from MCB iSSA emissions across the models. In section 4, we examine the processes causing model differences in ERF_{aci}. In section 5, we examine model differences in ERF_{ari}. Section 6 summarizes findings and discusses how future MCB simulations could be designed to enable better model inter-comparisons and process analysis.

While this analysis focuses on a detailed assessment of ESM representation of MCB aerosol-cloud interactions, we note that the underlying processes, biases, and limitations also apply to present-day inadvertent anthropogenic aerosol forcing. Cloud droplet activation, precipitation formation, and cloud entrainment effects are persistent sources of inter-ESM spread in aerosol forcing (Riipinen et al., 2026). Thus, improving ESM representations of MCB will likely improve present day aerosol-cloud forcing as well. Here, through the lens of MCB, we conduct a set of simulations that allows us to compare the full ERF curves across ESMs for a large range of emission rates, providing novel insights into the non-linearity of aerosol-cloud interactions at large scales and the processes that drive them.

https://doi.org/10.5194/egusphere-2026-5460
Preprint. Discussion started: 21 September 2026

2 Methods

2.1 Models and Simulations

We conduct a series of fixed sea surface temperature (SST) simulations in six ESMs to compute the effective radiative forcing (ERF) across a range of MCB iSSA emission rates in three subtropical regions with extensive low cloud cover. These regions are the Northeast Pacific (NEP: 0 to 30N and 170E to 120E), the Southeast Pacific (SEP: 30S to 0 and 120E to 70E), and the Southeast Atlantic (SEA: 30S to 0 and 25E to 15W), including only the grid boxes that are ≥50% ocean (Fig. 1a). While ESM studies indicate that MCB focused on the subtropical stratocumulus decks may produce undesirable remote climate effects (Rasch et al., 2009; Jones et al., 2009; Haywood et al., 2023; Odoulami et al., 2024; Chen et al., 2024b), these regions were selected to build on the existing dataset described in R2024, where subtropical regions were used to calibrate the MCB ERF. We note that inter-model differences in ERF_{aci} are similar regardless of emission region for three of the models (Hirasawa et al., 2026a), thus we assume that the findings here generalize to the midlatitude regions that have been the focus of more recent modeling (e.g., Chen et al., 2024a; Hirasawa et al., 2026b). The six ESMs in this study are:

CESM2 : Community Earth System Model version 2.1 (Danabasoglu et al., 2020) with the Community Atmosphere Model version 6 (CAM6) and Community Land Model 4.5 (CLM4.5). CAM6 uses the Morrison-Gettelman microphysics scheme version 2 (Gettelman and Morrison, 2015) in which SSA are activated following ARG2000. Autoconversion depends on N_d and condensation/evaporation depend on droplet radius following Khairoutdinov and Kogan (2000) (hereafter KK2000). SSA are represented in the Modal Aerosol Model 4 (MAM4) as internally mixed in Aitken, accumulation, and coarse aerosol modes (Liu et al., 2016). Natural SSA emissions are computed following Mårtensson et al. (2003) for 31 dry radius bins ranging from 20 nm to 23.7 μm. We introduce MCB iSSA emissions by adding half of the total number flux into each of two bins at dry radii 43 nm amd 52 nm, which are then mapped into the accumulation mode of the atmosphere model. We run CAM6 in the finite-volume grid with nominal 1-degree horizontal resolution with 32 vertical levels. Simulations are listed in Table S2.

E3SMv2 : Energy Exascale Earth System Model version 2.0 (Golaz et al., 2022) with Energy Atmosphere Model version 2 (EAMv2) and Energy Land Model version 2 (ELMv2). Like CAM6, EAMv2 uses the ARG2000 activation scheme and KK2000 autoconversion and condensation/evaporation schemes. However, a number of parameters that are critically important for determining the cloud response to MCB differ: EAMv2 has a higher minimum N_d, a wider (i.e. increased geometric standard deviation σ_g)accumulation mode in the modal aerosol model, removal of a lower limit on subgrid vertical velocity that is present in CAM6, reduced exponent coefficient for the autoconversion dependence on N_d, and higher vertical resolution in the boundary later. Together, these tend to reduce the susceptibility of clouds to aerosol (Ma et al., 2021; Golaz et al., 2022; Wan et al., 2025). We run EAMv2 in the cube-sphere grid at nominal 1-degree horizontal resolution with 72 vertical levels. The natural SSA emission parameterization is similar to CESM2, though E3SMv2 has overall higher fluxes due to an increase in SSA emission flux scaling and the addition of wind-driven organic aerosol

https://doi.org/10.5194/egusphere-2026-5460
Preprint. Discussion started: 21 September 2026

emissions. The MCB iSSA emissions are prescribed in the same way in the two models. Simulations are listed in Table S3.

CanAM5-PAM : Canadian Atmosphere Model version 5.1 (Sigmond et al., 2023) with the Piecewise log-normal Aerosol Model (PAM) (Von Salzen, 2006; Von Salzen et al., 2025), which represents aerosols by dividing the size spectrum into sections and representing the aerosol within each section using truncated log-normal distributions. The approach is based on an improved version of the Canadian Earth System Model version 5 (CanESM5) which replaces the standard bulk aerosol model with PAM. Aerosol activation is simulated using a quasi-steady state approximation of the droplet growth equation (Wang et al., 2022). To include MCB iSSA, we introduce an additional externally mixed mode that has the same chemical composition as natural SSA, but has a number mode radius of 50 nm and a geometric standard deviation of $\sigma = 1.6$. Autoconversion is computed using Wood et al. (2002) assuming a fixed climatological N_d concentration. The model resolution is T63 spectral with 49 vertical levels. Simulations are listed in Table S4.

UKESM1 : United Kingdom Earth System Model version 1.0 (Mulcahy et al., 2022) with the Unified Model Global Atmosphere version 7.1 (UM) and the Joint UK Land Environment Simulator (JULES) version 7.0 (Walters et al., 2019). The UM uses the modal version of the Global Model of Aerosol Processes (GLOMAP) in which SSA are included in the accumulation and coarse soluble aerosol modes. The model uses the ARG2000 activation scheme and the KK2000 autoconversion scheme (Mulcahy et al., 2020). Boundary layer entrainment is explicitly parameterized and can in principle respond to boundary layer instability caused by precipitation suppression (Walters et al., 2019). Natural SSA emissions are computed following Gong (2003). We introduce MCB iSSA emissions by adding the number flux into one bin with a dry radius of 86 nm, which is the most efficient size for this model (Haywood et al., 2023), and the aerosols are mapped into the accumulation mode of GLOMAP. We run UKESM1 at ~ 135km horizontal resolution with 85 vertical levels. Simulations are listed in Table S5.

NorESM2 : Norwegian Earth System Model version 2 (Seland et al., 2020) with the Norwegian version of CAM6 (CAM6-Nor) and Community Land Model version 5 (CLM5). CAM6-Nor is branched from CAM6 and incorporates differences in the aerosol scheme, aerosol-cloud interactions, and moist convection, among other processes. Aerosols are represented using the OsloAero model (Kirkevåg et al., 2018), which is a modal scheme that includes tagging for aerosol production and transformation processes. SSA are represented in Aitken, accumulation, and coarse aerosol modes, whose properties are modified in the atmosphere when processed to become aerosol "mixtures". Size-resolved microphysical properties such as aerosol optical properties are calculated offline. The cloud microphysics module is the same as in CAM6, and thus the model uses ARG2000 activation and KK2000 autoconversion (the Morrison-Gettelman version 2, Gettelman and Morrison (2015)). Natural SSA emissions are computed following Salter et al. (2015) and emission rates are computed for the three main sea salt aerosol modes. We introduce MCB iSSA emissions by adding number flux into the Aitken mode of the parameterization, which corresponds to aerosol with an approximate volume radius of 108 nm and modal radius of 47.3 nm. We run NorESM2 at $\sim 2°$ resolution with 32 vertical levels. Simulations are listed in Table S6.

https://doi.org/10.5194/egusphere-2026-5460
Preprint. Discussion started: 21 September 2026

GFDL-AM4 : Geophysical Fluid Dynamics Laboratory Atmosphere Model v4 with Land Model v4 (Zhao et al., 2018). SSA are represented with five size bins and natural SSA emissions are computed following Mårtensson et al. (2003) for aerosol smaller than 1.4 μm and the Monahan et al. (1986) for particles larger than 1.4 μm. The Ming et al. (2007) parameterization is used for cloud activation and autoconversion depends on N_d following Rotstayn (1997). MCB iSSA are emitted into the smallest size bin (0.1-0.5 μm) available in the natural SSA emission parameterization. We run GFDL-AM4 on a cube-sphere grid with approximately 100 km grid size and 33 vertical levels. Simulations are listed in Table S7.

We further conduct simulations in four of the models with modified parameterizations to explore how specific processes influence the MCB ERF:

CanAM5-PAM-Adj : CanAM5-PAM simulations in which we introduce a dependence of autoconversion rate on N_d following Wood et al. (2002). Simulations are listed in Table S8.

CESM2-Ghosh : We conduct simulations in CESM2 with an adjusted version of the ARG2000 activation parameterization from Ghosh et al. (2025) (CESM2-Ghosh). Ghosh et al. (2025) modified the parameters in the ARG activation parameterization to account for kinetic limitations on droplet activation, which prevents suppression of the CCN activation at unrealistically low N_d concentrations. In the unadjusted ARG2000 parameterization this can occur at CCN concentrations as low as 1000 cm^{-3}, substantially lower than the 10^4 cm^3 at which this occurs in parcel models (Fig. 4a). Adjustments to correct this limitation have been recommended to improve the performance of ARG2000 in cases with high concentrations of small aerosol particles (Riipinen et al., 2026). Such conditions are likely to occur in MCB deployment regions, and the Ghosh et al. (2025) modification to the parameterization tend to increase the activation rate in these conditions. For CESM2, we update the ARG2000 parameters using geometric standard deviation $\sigma_g = 1.6$. Parameter changes are shown in supplemental text 1. Simulations are listed in Table S9.

E3SMv2-Ghosh : E3SMv2 simulations with ARG2000 parameters updated following Ghosh et al. (2025) (Text S1) using geometric standard deviation $\sigma_g = 1.8$. Simulations are listed in Table S10.

UKESM1-Ghosh : UKESM1.1 simulations with ARG2000 parameters updated following Ghosh et al. (2025) (Text S1) using geometric standard deviation $\sigma_g = 1.4$. Details are listed in Table S11.

Table 1 summarizes the iSSA emission particle size, the activation parameterization, autoconversion parameterization, and the natural SSA parameterization used in each model. Figure 1b,c show the log-normal mass and number distributions of the emitted iSSA particles in each model, assuming equal total number flux in each model, showing the large variations in emitted mass depending on width and modal radius of the distributions. The emission rates used in each simulation, the length of the simulations, and the background conditions differ across the models and are summarized in Tables S1 to S6 for the different models.

We note that the activation scheme used by GFDL-AM4 assumes a fixed sea salt aerosol size distribution and maps the SSA mass into this distribution (Zhao et al., 2018). As a result, the MCB iSSA size distribution is shifted to larger sizes more

https://doi.org/10.5194/egusphere-2026-5460
Preprint. Discussion started: 21 September 2026

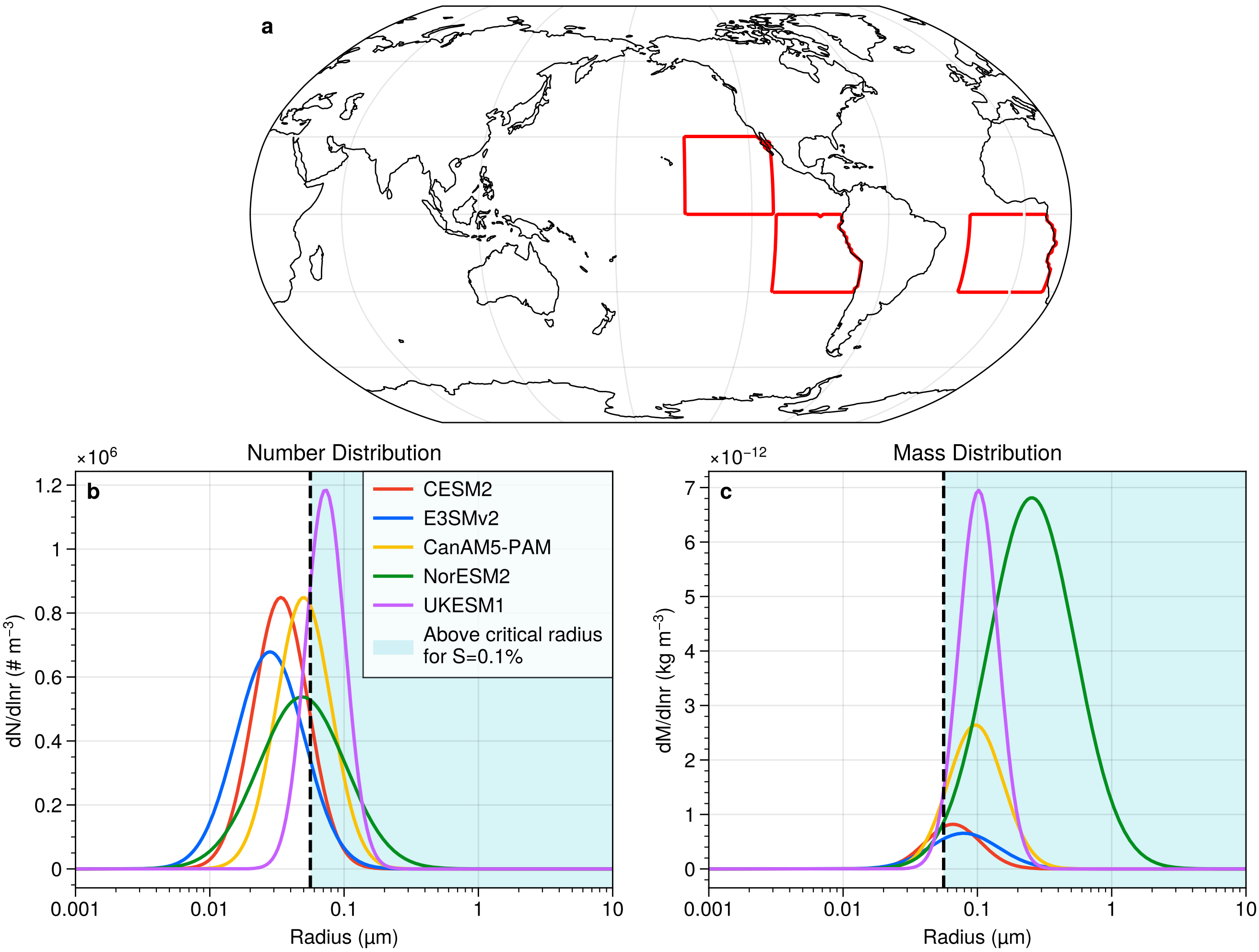

Figure 1. Northeast Pacific (NEP: 0 to 30N and 170E to 120E), Southeast Pacific (SEP: 30S to 0 and 120E to 70E), and Southeast Atlantic (SEA: 30S to 0 and 25E to 15W) iSSA emission regions used in this study (a). Log-normal Number (b) and Mass (c) distributions of emitted iSSA particles for the different models where the total number concentration is $N_0 = 1\mathrm{cm}^{-3}$ in each. Distribution widths are computed using the geometric standard deviation of the accumulation SSA mode in each model. Dashed vertical line and blue shading shows the critical radius for cloud condensation nuclei at supersaturation S=0.1%.

suitable for natural SSA, meaning the iSSA number concentration seen by the activation scheme becomes erroneously low. We nevertheless include GFDL-AM4 results in Fig. 2 and 3 despite these deficiencies, because it has been used in the past to estimate MCB ERF (Mahfouz et al., 2023) and it is important to place those results in the wider context of the ESM ensemble. However, we exclude it from the subsequent analyses.

https://doi.org/10.5194/egusphere-2026-5460
Preprint. Discussion started: 21 September 2026

Model	iSSA volume radius	iSSA median radius	σ_g	Natural SSA parameterization	Activation parameterization	Autoconversion parameterization	CCN Fraction at S=0.1%
CESM2	47.1nm	33.8nm	1.6	Mårtensson et al. (2003)	ARG2000	KK2000*	0.157
CESM2-Ghosh	47.1nm	33.8nm	1.6	Mårtensson et al. (2003)	Ghosh et al. (2025)	KK2000*	0.157
E3SMv2	47.1nm	28.1nm	1.8	Mårtensson et al. (2003)	ARG2000	KK2000†	0.131
E3SMv2-Ghosh	47.1nm	28.1nm	1.8	Mårtensson et al. (2003)	Ghosh et al. (2025)	KK2000†	0.131
CanAM5-PAM	86.9nm	62.6nm	1.6	Ma et al. (2008)	Wang et al. (2021)	Wood et al. (2002) Fixed N_d	0.445
CanAM5-PAM-Adj	86.9nm	62.6nm	1.6	Ma et al. (2008)	Wang et al. (2021)	Wood et al. (2002) with N_d change	0.445
UKESM1	85.9nm	72.5nm	1.4	Gong (2003)	ARG2000	KK2000*	0.805
UKESM1-Ghosh	85.9nm	72.5nm	1.4	Gong (2003)	Ghosh et al. (2025)	KK2000*	0.805
NorESM2	108nm	47.3nm	2.1	Salter et al. (2015)	ARG2000	KK2000*	0.420
GFDL-AM4	300nm	N/A	N/A	Mårtensson et al. (2003)	Ming et al. (2007)	Rotstayn (1997)	0.141

Table 1. Earth System Models used in this study, the volume radii (mass flux divided by number flux), median radii (typical radii of the aerosols), and geometric standard deviation of the lognormal iSSA distributions used for MCB, the natural SSA parameterization, the activation parameterization, autoconversion parameterization, and the fraction of aerosol particles that are cloud condensation nuclei at $S = 0.1\%$. * KK2000 with parameters $(\frac{dq_r}{dt})_{auto} = 1350 q_c^{2.47} N_c^{-1.79}$. For rain water content q_r and cloud water content q_c. † KK2000 with parameters $(\frac{dq_r}{dt})_{auto} = 30500 q_c^{3.19} N_c^{-1.2}$.

2.2 Analysis

We use the approximate partial radiative perturbation (APRP) method to estimate the direct aerosol (ERF_{ari}) and aerosol-cloud (ERF_{aci}) forcing components of the iSSA total ERF (ERF_{tot}) (Zelinka et al., 2023). Grid-average CCN and in-cloud N_d concentrations are computed at cloud base and cloud top, respectively. We define cloud base as the lowest vertical level at which the liquid cloud fraction increases above 0.05 and the cloud top as the vertical level at which the liquid cloud fraction is greatest in the column. These values are computed using monthly mean fields, which means we neglect sub-monthly and sub-grid covariances between CCN, N_d, and cloud cover/height.

To estimate the flux of CCNs, we estimate the fraction of activated particles for $S = 0.1\%$ following the Köhler theory implementation for a lognormal distribution in the pyrcel package (Rothenberg and Wang, 2016). We choose $S = 0.1\%$ as it is the default supersaturation used for CCN output in CESM2, E3SMv2, and NorESM2. For CanAM5-PAM and CanAM5-PAM-Adj, we have the CCN concentrations at $S = 0.2\%$. In order to estimate CCN at $S = 0.1\%$, we multiply the original CCN at $S = 0.2\%$ by the ratio of the number of activated particles for $S = 0.1\%$ versus the number of activated particles for $S = 0.2\%$ (~ 1.84), as the activation fraction scales approximately linearly for these supersaturations.

https://doi.org/10.5194/egusphere-2026-5460
Preprint. Discussion started: 21 September 2026

We estimate the aerosol mass lifetime of accumulation mode MCB iSSA by assuming the MCB iSSA mass burden is a product of the emission flux and the iSSA mass lifetime $M_{MCB} = \tau_{MCB} F_{MCB}$ and assuming a constant climatological SSA burden M_{clim}. By considering the change in total SSA burden (M_{tot}) as the iSSA mass flux (F_{MCB}) increases we have

$$M_{tot} = M_{clim} + M_{MCB} = M_{clim} + \tau_{MCB} F_{MCB} \quad (1)$$

Thus, after computing the linear regression of the total iSSA burden against the iSSA mass flux, the slope approximates the lifetime associated with the MCB iSSA (τ_{MCB}).

Because the models use different emission rates, we quantitatively compare them by interpolating ERF_{tot} by assuming the following functional forms for ERF_{aci} and ERF_{ari} dependence on the iSSA mass flux M_{ssa}:

$$ERF_{aci} \approx a \ln(1 + bM_{ssa})$$

$$ERF_{ari} \approx cM_{ssa}$$

where we calculate a, b, and c by fitting to the ERF_{aci} and ERF_{ari} values diagnosed using APRP. For ERF_{aci}, we restrict the fit to simulations with < 100 Tg yr^{-1} iSSA emissions. The resulting fitting parameters and curves are shown in Table **??** and Fig. **??**. The logarithmic form of ERF_{aci} follows Stevens (2015). These fits function well for low emission rates, where the logarithmic form of ERF_{aci} approximately holds, and for very high emission rates, where ERF_{ari} dominates and is well characterized by a linear fit. The logarithmic fit tends to overestimate the actual ERF_{aci} at higher emission rates in large part because the ARG activation scheme used in most of the models predicts incorrectly that additional iSSA will decrease N_d at higher emission rates (discussed in more detail in section 4). However, we argue the fits allow reasonable interpolation at the emission and forcing levels we discuss in the following paragraphs (Fig. **??**).

3 Effective radiative forcing

There are major differences across the ESMs in ERF_{tot} due to iSSA (Fig. 2a; Table 2), even when excluding the erroneously weak GFDL-AM4 ERF_{aci}. Based on the interpolated curves (Fig. S1), we find that ERF_{tot} at a global sum mass emission rate of 30 Tg yr^{-1}varies from -0.89 Wm^{-2} (NorESM2) to -3.97 Wm^{-2} (CanAM5-PAM-Adj). Conversely, to achieve a global mean ERF_{tot} of -2 Wm^{-2}, the models require iSSA mass fluxes ranging from 7.21 Tg yr^{-1} (CESM2-Ghosh) to 95.7 Tg yr^{-1} (UKESM1). Notably, differences in the iSSA emission size distributions prescribed at the surface play an important role in determining the forcing sensitivity per emitted mass, and thus the inter-model range is not necessarily related to structural uncertainties in the models. We account for these differences by comparing the ERF_{tot} against the total iSSA number flux emissions (Fig. 2b). This reduces the inter-model spread, particularly at lower emission rates (e.g., UKESM1 and NorESM2 fall within the range of the other models once the emitted aerosol size is accounted for). At a number flux rate of 5 $\times 10^{20}$ s^{-1}, which corresponds to 30 Tg yr^{-1} for the CESM2 and E3SMv2 iSSA size distributions, the ERF_{tot} range shifts, ranging from -0.93 Wm^{-2} (E3SMv2) to -4.96 Wm^{-2}(CanAM5-PAM-Adj), with different end-member models. To achieve $ERF_{tot} = -2$ Wm^{-2}, the models require total number fluxes of 0.77 $\times 10^{20}$ s^{-1} and 23.9 $\times 10^{20}$ s^{-1}, respectively.

https://doi.org/10.5194/egusphere-2026-5460
Preprint. Discussion started: 21 September 2026

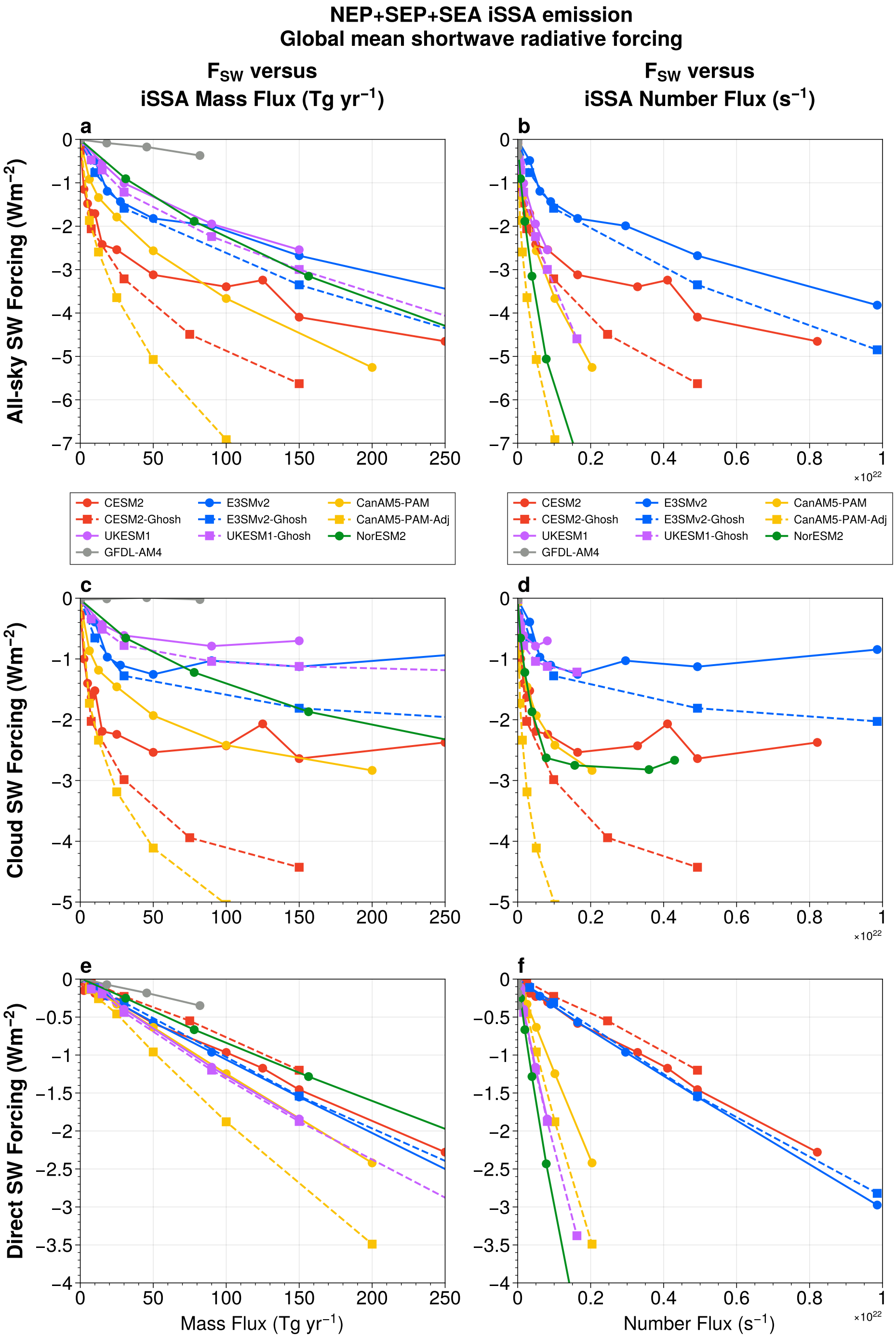

Figure 2. Annual global mean anomalies of shortwave ERF_{aci} (a, b), shortwave ERF_{ari} (c, d), and shortwave ERF_{tot} (e,f) for different SSA emission rates in the ten models considered here. First column shows the forcing versus SSA mass flux (a,c,e) and second column shows the forcing versus SSA number flux (b,d,f).

https://doi.org/10.5194/egusphere-2026-5460
Preprint. Discussion started: 21 September 2026

Much of the inter-model spread in ERF_{tot} arises from a spread in ERF_{aci} (Fig. 2c,d; Table 2). While there is a range in ERF_{aci} susceptibility at low emission rates, the bulk of the inter-model spread arises from differences in the saturation forcing. Across all models, we see that ERF_{aci} plateaus at higher emission rates and in CESM2, E3SMv2, and NorESM2 even enter a regime in which additional SSA reduces the ERF_{aci} (although the net ERF_{tot} still increases due to the direct aerosol effect). The strong saturation behaviour seen in these models is an artifact of the ARG2000 activation parameterization, as discussed in detail in section 4. However we note forcing quasi-saturation is a general feature of the Twomey effect, arising from reduced activation efficiency at high N_d concentrations. The models show a range in saturation forcing from $F_{cld} = -0.8$ Wm^{-2} to $F_{cld} = -3.3$ Wm^{-2}. The flux at which the forcing saturates also varies, with E3SMv2 saturating at ~50 Tg yr^{-1} ($\sim 0.5 \times 10^{21}$ s^{-1}) while CanAM5-PAM has not completely saturated even at >200 Tg yr^{-1} ($\sim 5 \times 10^{21}$ s^{-1}). Thus, the inter-model spread in MCB ERF_{tot} appears to be dominated by the limitations in aerosol activation, especially at intermediate emission rates where saturation is important but the ERF_{ari} does not yet dominate.

All of the models used here (except GFDL-AM4) show that ERF_{aci} accounts for the majority of the forcing for at least some of the emission rates tested (Fig. S2). At high emission rates ERF_{aci} saturates and ERF_{tot} becomes dominated by ERF_{ari}. We see monotonic increases in ERF_{tot} with mass emission rate in all models due to ERF_{ari}, even in the models which simulate reductions in ERF_{aci} at high emission rates. The point at which the forcing switches from ERF_{aci}-dominated to ERF_{ari}-dominated differs across models. In UKESM1 this occurs when the $ERF_{tot} = -1$ Wm^{-2}, while for CanAM5-PAM-Adj the cloud forcing accounts for the majority of forcing even as the ERF_{tot} exceeds -10 Wm^{-2}.

4 Aerosol-cloud interactions

ERF_{aci} differences across the models are driven by a series of relationships which we aim to encapsulate in Fig. 3:

(a) CCN at $S = 0.1\%$ at cloud base versus CCN surface number flux : Captures information about the iSSA lifetime, and vertical mixing to cloud base. The iSSA lifetime and mixing depend on model differences in iSSA deposition, turbulence, and iSSA size distribution.

(b) N_d at cloud top versus CCN at $S = 0.1\%$: Captures information about CCN activation into cloud droplets. This depends on model differences in activation parameterizations, sub-grid updrafts from turbulence schemes, and low cloud fraction.

(c) N_d at cloud top versus CCN surface number flux : Combines information from panels (a) and (b) to allow comparisons with UKESM1 and GFDL-AM4, for which we do not have CCN data.

(d) cloud fraction versus N_d at cloud top : Captures information about the strength of the aerosol precipitation suppression effect on cloud fraction. This depends on model differences in how autoconversion and dry-air turbulent entrainment depend on N_d.

(e) total grid liquid water path (LWP) versus N_d at cloud top : Captures information about how aerosol precipitation suppression affects cloud liquid water content, which depends on the same processes as (d).

https://doi.org/10.5194/egusphere-2026-5460
Preprint. Discussion started: 21 September 2026

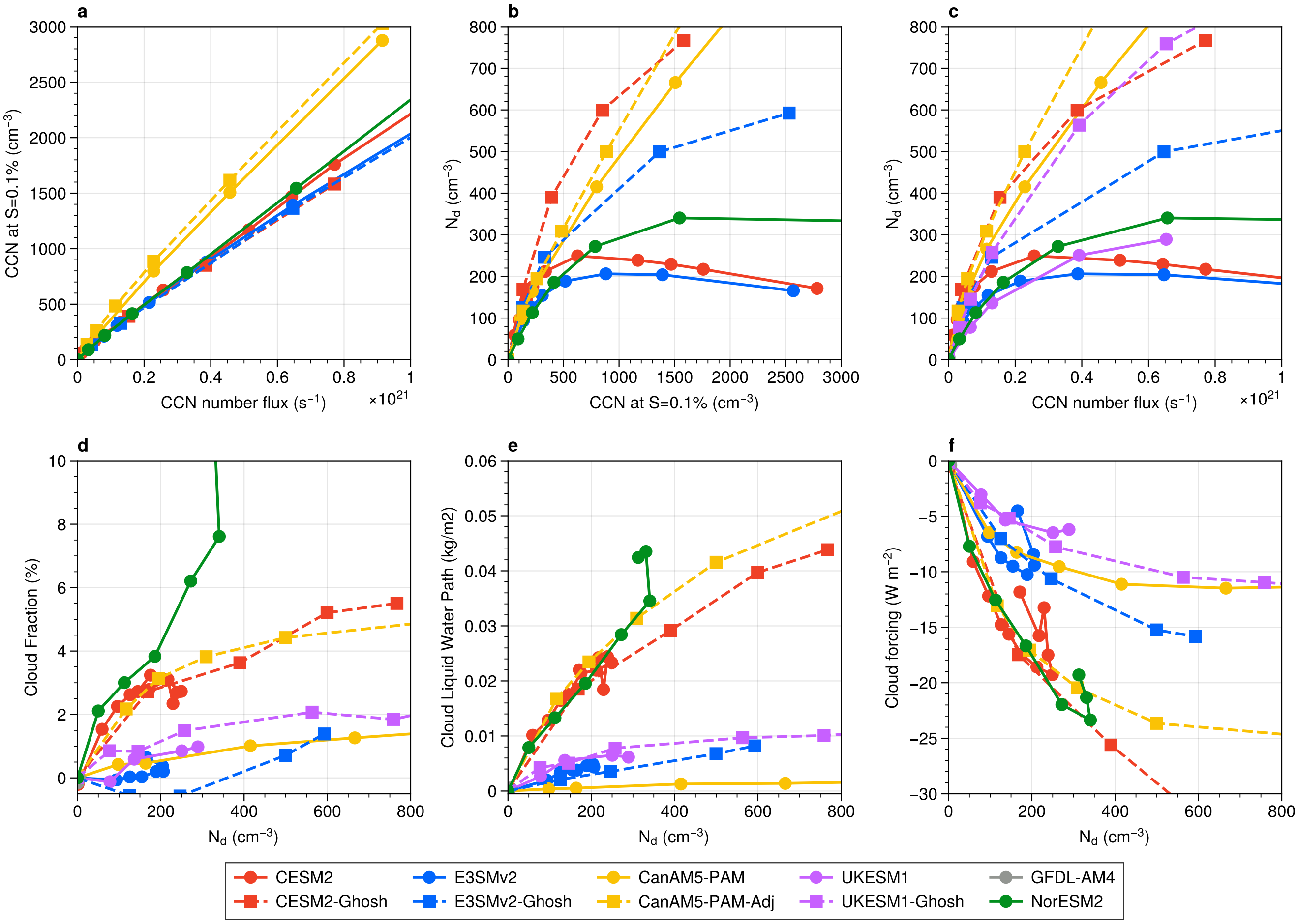

Figure 3. Annual mean anomalies averaged over the NEP, SEP, and SEA emission regions across different models. Each panel captures some aspect of the aerosol-cloud interaction: a) aerosol lifetime and mixing to cloud base (CCN at $S = 0.1\%$ vs. CCN number flux), b) aerosol activation (N_d vs. CCN at $S = 0.1\%$), c) aerosol lifetime, mixing, and activation (N_d at cloud base vs. CCN number flux), d) cloud lifetime effect (cloud fraction vs. N_d), e) cloud liquid water effect (LWP vs. N_d), and f) total aerosol indirect effect (APRP cloud forcing vs. N_d). Note that GFDL-AM4 is displayed in panels c, d, e, and f, but is not visible due to the small N_d anomalies in this model.

https://doi.org/10.5194/egusphere-2026-5460
Preprint. Discussion started: 21 September 2026

Model	ERF_{tot} at 30 Tg yr^{-1} (Wm^{-2})	ERF_{tot} at 5×10^{20} s^{-1} (Wm^{-2})	Mass flux for ERF_{tot}= -2 Wm^{-2} (Tg yr^{-1})	Number flux for ERF_{tot}= -2 Wm^{-2} (10^{20} s^{-1})	Slope of ERF_{ari} Wm^{-2}(Tg yr^{-1})$^{-1}$
CESM2	-2.62	-2.11	12.9	4.25	-0.0121
E3SMv2	-1.27	-0.93	75.4	24.8	-0.0106
CanAM5-PAM	-1.99	-2.48	30.4	3.10	-0.0122
UKESM1	-0.96	-1.95	95.7	5.18	-0.0124
NorESM2	-0.89	-3.66	85.73	2.15	-0.00827
GFDL-AM4	-0.131	-24.7	457.1	0.40	-0.00420
CESM2 (Ghosh ARG)	-3.34	-2.66	7.21	2.37	-0.00785
E3SMv2 (Ghosh ARG)	-1.59	-1.02	44.20	14.5	-0.0104
UKESM1 (Ghosh ARG)	-1.52	-0.935	59.95	44.2	-0.0108
CanAM5-PAM (w/ Adjustments)	-3.97	-4.93	7.62	0.78	-0.0178

Table 2. ERF_{tot} at selected mass (30 Tg yr^{-1}) and number (5×10^{20} s^{-1}) fluxes for each model, mass and number flux to achieve ERF_{tot}= -2 Wm^{-2} for each model, and the slope of ERF_{ari} vs. mass emissions for each model. Values are computed by fitting to $F_{tot} = F_{cld} + F_{aer} = a\ln(bM_{ssa}) + cM_{ssa}$.

(f) APRP-derived SW cloud forcing versus N_d at cloud top : Captures the total SW forcing response to cloud droplet increases, encompassing aerosol effects on cloud albedo (Twomey effect and LWP effect) and cloud lifetime (cloud fraction effect).

The fraction of iSSA that are CCN at $S = 0.1\%$ differs by a factor of five between CanAM5-PAM and E3SMv2 (Fig. S3b). This is mainly due to differences in the emitted iSSA size distribution. The choice of supersaturation ($S = 0.1\%$) corresponds to a critical radius of ~ 56nm. Thus, for a given total iSSA number flux, CanAM5-PAM and NorESM2 produce higher CCN concentrations because a larger fraction of their emitted particles exceeds this critical radius (Fig. 1b). After accounting for the fraction of iSSA that are CCN, the spread in the CCN concentration scaling is substantially reduced (Fig. 3a, Fig. S3c). There are additional differences driven by differences in aerosol lifetime, which depends on differences in aerosol deposition and vertical mixing. For example, iSSA lifetimes are about 4 days for CanAM5-PAM and 7 days for CanAM5-PAM-Adj (section 5), which results in slightly larger CCN concentrations in the latter.

The activation rates across the models are similar for regional average CCN concentrations below $\sim$400 cm^{-3}, but they diverge substantially at higher concentrations (Fig. 3b) for the seven models where we have CCN data. Taking a more detailed look in Figure 4, we can see that at ~ 1000 cm^{-3}, E3SMv2 has $N_d \approx 250$ cm^{-3} (or $\sim$25% activated fraction, Fig. 4c) while

https://doi.org/10.5194/egusphere-2026-5460
Preprint. Discussion started: 21 September 2026

CESM2-Ghosh has $N_d \approx 650$ cm^{-3} (or ∼65% activated fraction, Fig. 4b), a $\sim 2.5\times$ difference. This range increases further at higher emission rates, as models with the default ARG2000 activation parameterization (CESM2, E3SMv2, NorESM2) saturate and even simulate declining N_d above CCN concentrations of 1000 cm^{-3} due to unrealistically strong suppression of CCN activation (Connolly et al., 2014; Ghosh et al., 2025). CESM2 and E3SMv2 saturate at a lower CCN concentration than NorESM2, which may be due to the smaller emitted iSSA size in these models. Use of the ARG2000 parameterization with updated parameter values (CESM2-Ghosh, E3SMv2-Ghosh) and the Wang activation scheme (CanAM5-PAM, CanAM-PAM-Adj) both produce continued increases in N_d well past those concentrations.

The CESM2, E3SMv2, and NorESM2 results align with previous NorESM work which showed a maximum achievable N_d of ∼400 cm^{-3}(Alterskjaer and Kristjánsson, 2013), also using the ARG2000 parameterization. However, the CESM2-Ghosh, E3SMv2-Ghosh, UKESM1-Ghosh and CanAM5-PAM results suggest much higher N_d concentrations are possible. Saturation occurs at $N_d > 800$ cm^{-3}in these models, which is more consistent with cloud resolving model (Jenkins et al., 2013) and parcel model estimates (Connolly et al., 2014). Combining these two relationships to compare N_d to CCN number flux (Fig. 3c), we see that UKESM1 also falls well within the model spread. Together, these indicate that at low iSSA concentrations, activation rates are similar across the models while at high iSSA concentrations, activation becomes a major source of inter-model spread. The saturation of ERF_{aci} appears to be mainly controlled by these limits on aerosol activation at high concentrations; thus, constraining this upper activation limit is important for estimating the MCB forcing at these high iSSA emission rates.

We see further inter-model differences arising from cloud adjustments (Fig. 3d, e). E3SMv2, E3SMv2-Ghosh, CanAM5-PAM, and UKESM1 (models with smaller cloud adjustments) show weak cloud liquid water path (LWP) responses to N_d changes while CESM2, CESM2-Ghosh, NorESM2, and CanAM5-PAM-Adj (high adjustment models) show consistent increases in cloud liquid water content and cloud fraction with N_d (Fig. 3e, f). Binning the cloud fraction (Fig. 5) and LWP (Fig. S5) responses by N_d, we see more distinctly that CESM2, CESM2-Ghosh, and NorESM2 have very strong cloud adjustments and are similar to one another due to their shared autoconversion parameterization and tuning for that parameterization (Fig. 5a,b,g). CanAM5-PAM-Adj also simulates CF and LWP increases (Fig. 5f), though they are not as strong as with CESM2. The cloud fraction and LWP vary similarly with respect to N_d across the models (Fig. S5), in part because the LWP is grid-averaged and thus CF increases tend to also increase LWP. However, even when accounting for CF changes, LWP still increases, meaning that the clouds become simultaneously thicker and more extensive in the models with stronger adjustments. This contrasts with observational estimates of cloud adjustments, which show that aerosol perturbations tend to cause neutral or decreased LWP within clouds (Coakley Jr and Walsh, 2002; Ackerman et al., 2004; Bender et al., 2019; Mülmenstädt et al., 2024).

CanAM5-PAM's weaker cloud adjustments (Fig. 5e) are due to structural differences, as the model computes the autoconversion rate assuming a fixed N_d. For E3SMv2 they are due to model tuning (Fig. 5c,d): E3SMv2 uses an autoconversion parameterization identical to that in CESM2 and NorESM2 but in E2SMv2 it has been tuned to substantially weaken its dependence on N_d (Golaz et al., 2022). UKESM1 also uses the same KK2000 autoconversion parameterization as CESM2 and NorESM2. Thus, we may expect to see similarly strong precipitation suppression. The fact that it shows weak cloud adjustments indicates other processes, such as entrainment changes, offset the cloud thickening effect of precipitation suppression,

https://doi.org/10.5194/egusphere-2026-5460
Preprint. Discussion started: 21 September 2026

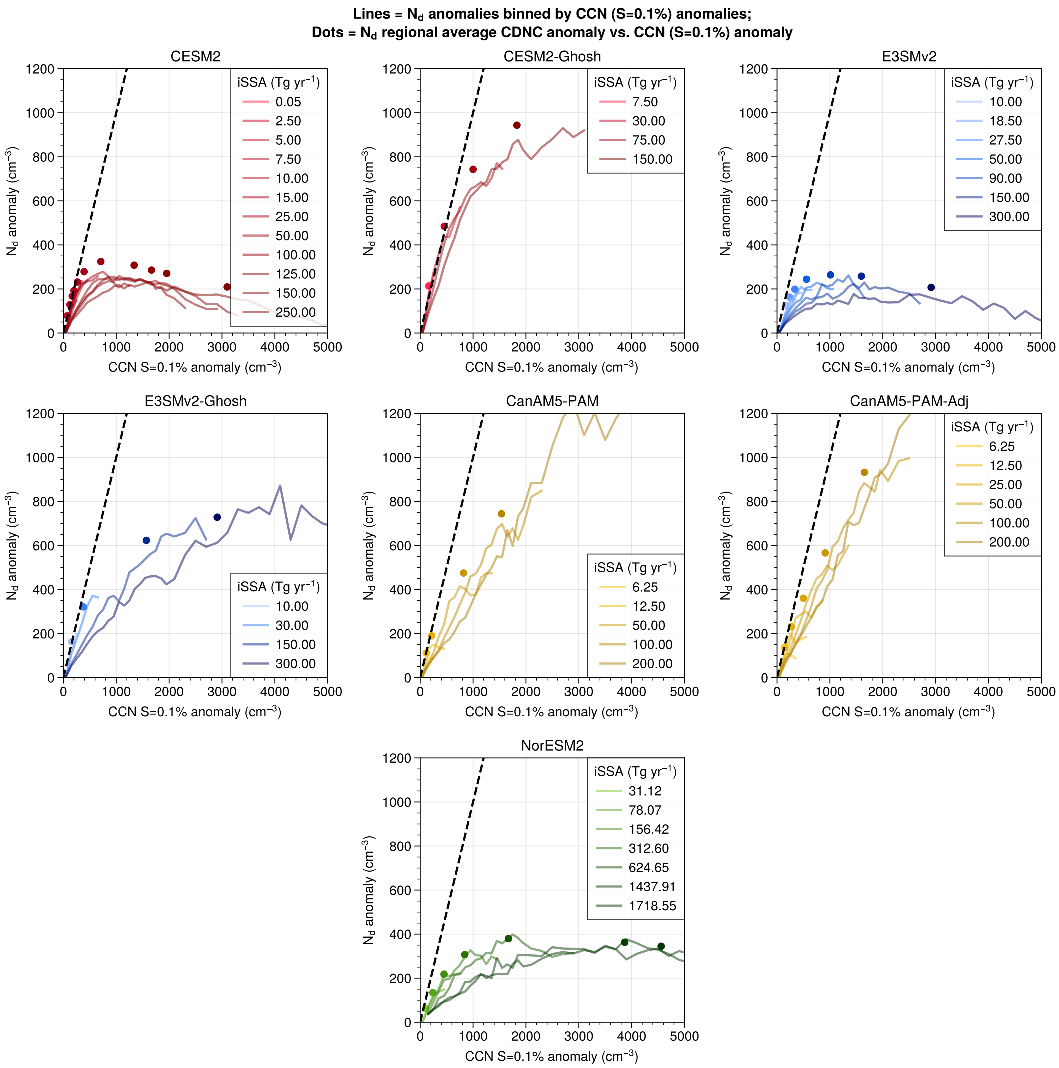

Figure 4. Time-mean N_d anomalies bin-averaged across spatial grid points by the time-mean CCN anomaly, in CESM2 (a), CESM2-Ghosh (b), E3SMv2 (c), E3SMv2-Ghosh (d), CanAM5-PAM (e), CanAM5-PAM-Adj (f), and NorESM2 (g). Intensity of the line colours indicates the iSSA emission rate, with lighter colours corresponding to lower emission rates and darker colours corresponding to higher emission rates. We omit CCN bins that contain fewer than 0.1% of grid points. Dots show the regional average anomalies for the Southeast Pacific (SEP) region, defined as 30S to 0 and 120E to 70E. Due to data limitations, we omit UKESM1 for this figure. Black dashed line shows the one-to-one line.

https://doi.org/10.5194/egusphere-2026-5460
Preprint. Discussion started: 21 September 2026

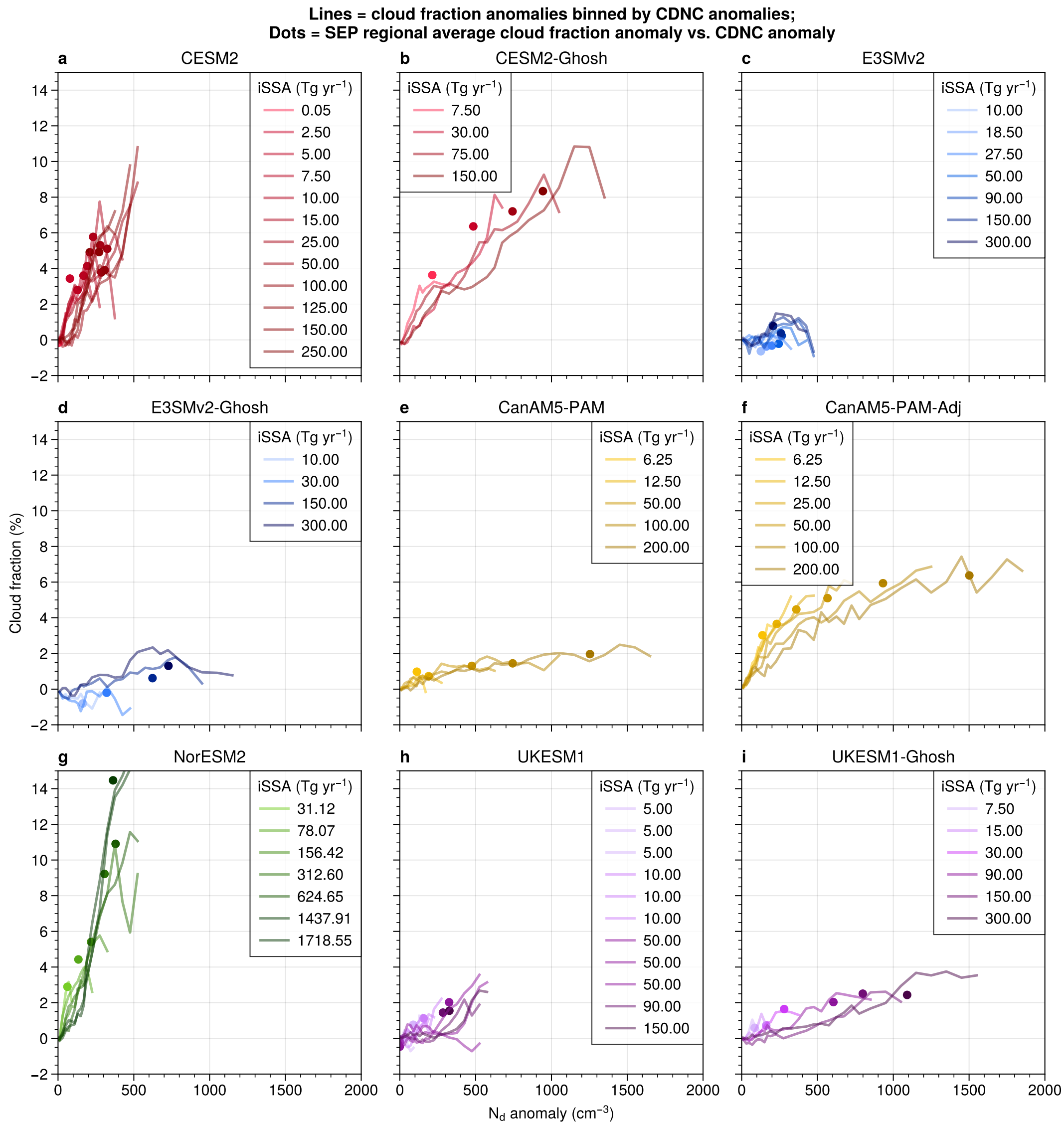

Figure 5. Time-mean grid-box cloud fraction anomalies bin-averaged across spatial grid points by the time-mean N_d anomaly for CESM2 (a), CESM2-Ghosh (b), E3SMv2 (c), E3SMv2-Ghosh (d), CanAM5-PAM (e), CanAM5-PAM-Adj (f), and NorESM2 (g). Intensity of the line colours indicates the iSSA emission rate, with lighter colours corresponding to lower emission rates and darker colours corresponding to higher emission rates. We omit N_d bins that contain fewer than 0.1% of the grid points. Dots show the regional average anomalies for the Southeast Pacific (SEP) region, defined as 30S to 0 and 120E to 70E.

reducing the cloud adjustment strength. We see weakly positive average CF adjustments in the low-adjustment models as well (Fig. 5c,d,e,h). Thus, while the precipitation suppression effect is substantially weakened, it seems to still occur to some extent.

https://doi.org/10.5194/egusphere-2026-5460
Preprint. Discussion started: 21 September 2026

Inter-model differences in how ERF_{aci} depends on N_d is largely driven by these differences in cloud adjustments (Fig. 3f). The models fall into two groups following the cloud adjustment strengths: CESM2, CESM2-Ghosh, NorESM2, and CanAM5-PAM-Adj show higher ERF_{aci} susceptibility and UKESM1, E3SMv2, E3SMv2-Ghosh, and CanAM5-PAM show lower ERF_{aci} susceptibility. Figure 6 shows the total SW cloud forcing as well as the forcing due only to the change in cloud amount for each model grid point, binned by the N_d anomaly of each grid point. The majority of the ERF_{aci} is from an increase in cloud albedo (Twomey effect and LWP changes), even in models with larger cloud fraction changes.

All eight models show a reduction of ERF_{tot} per ΔN_d at higher iSSA emission rates, as indicated by the shallower slopes of the binned averages. This is firstly due to the spatial distribution of low clouds, which decreases going west from the three emission regions. As emissions increase, more aerosol is transported west along the climatological trade winds into these less cloudy regions, because the grid-box average ERF_{aci} is generally weaker if there are fewer clouds. In Fig. S7, which shows analytic estimates of the Twomey forcing, we see that the forcing curve at different emission rates become similar if we assume a uniform cloud fraction for both CESM2, CESM2-Ghosh, E3SMv2, and E3SMv2-Ghosh. There is also a secondary effect from the interaction between the ERF_{ari} and ERF_{aci}. Increasing ERF_{ari} above the clouds decreases the transmissivity of the free troposphere (Fig. S6), which reduces the forcing effect of cloud albedo increases. Thus, accounting for this change in free troposphere transmissivity decreases ERF_{aci} for a given N_d perturbation, bringing the Twomey effect estimates slightly closer to the real model results in Fig. S7. However, we have not quantified the effect of relative increases in the diffuse versus direct radiation flux, which may increase the scattering by low clouds (Gristey and Feingold, 2025), which may offset this effect.

These effects have two interesting consequences: reductions in cloud albedo forcing even when activation is not saturated in CanAM5-PAM (Fig. 6e,f) and "fishhooks" in ERF_{aci} at high N_d values in CESM2, E3SMv2, and NorESM2 (cases where two simulations can have similar N_d anomalies, but the higher emission rate case sees lower forcing - Fig. 3f; Fig. 6a,c,g). This "fishhook" behaviour results from a combination of the unrealistically strong activation suppression in the ARG2000 scheme and the reduced forcing efficiency of higher emission rate cases, resulting in a situation where not only do activation rates decrease as iSSA emissions increase, but the albedo change is reduced for the activated particles as well. This fishhook behaviour does not occur in models with the Ghosh ARG2000 parameter changes (Fig. 6b,d,i) because increased droplet activation increases forcing faster than the transport and transmissivity effects decrease it. It may occur in UKESM1, but we have not tested sufficiently high emission rates to see this behaviour (Fig. 6h). This reduced efficiency is clearest when looking at the grid-point-wise forcing. In the global mean (Fig. S4f), the grid-point efficiency reductions are offset by the fact that as iSSA emissions increase, aerosol transport means an increasingly large region will see significant CCN enhancements and there will be a larger region of brightening. Thus, the saturation of forcing is less severe in the global mean, emphasizing the importance of aerosol deposition and transport in determining MCB efficacy.

https://doi.org/10.5194/egusphere-2026-5460
Preprint. Discussion started: 21 September 2026

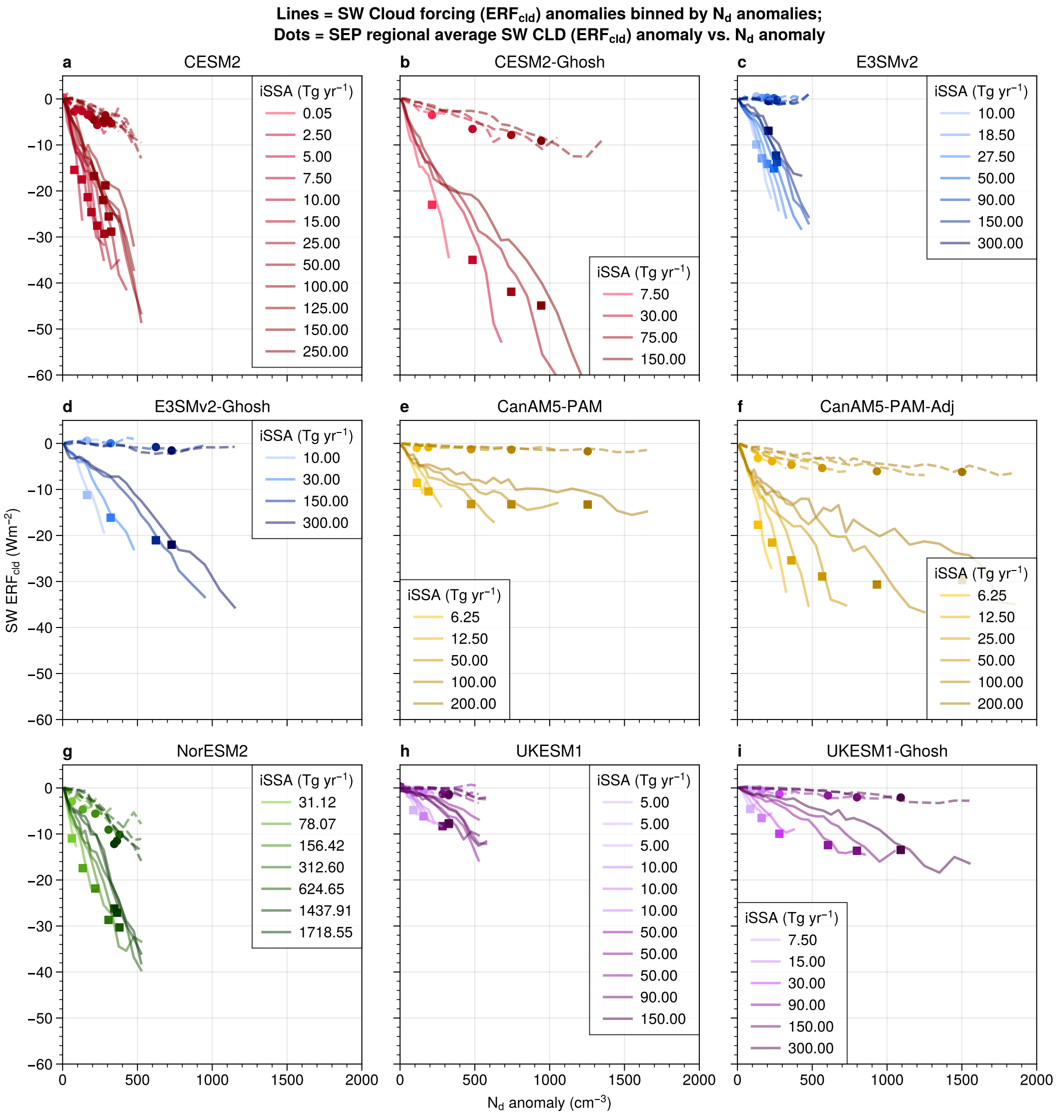

Figure 6. Time-mean total cloud forcing (solid lines) and cloud amount forcing (dashed lines), bin-averaged across spatial grid points by the time-mean N_d anomaly, for CESM2 (a), CESM2-Ghosh (b), E3SMv2 (c), E3SMv2-Ghosh (d), CanAM5-PAM (e), CanAM5-PAM-Adj (f), and NorESM2 (g). Cloud forcing and cloud amount forcing are diagnosed using APRP. Intensity of the line colours indicate the iSSA emission rate, with lighter colours corresponding to lower emission rates and darker colours corresponding to higher emission rates. We omit CCN bins that contain fewer than 0.1% of grid points. Dots show the regional average anomalies for the Southeast Pacific (SEP) region, defined as 30S to 0 and 120E to 70E.

https://doi.org/10.5194/egusphere-2026-5460
Preprint. Discussion started: 21 September 2026

5 Direct Aerosol forcing

We see a smaller but still substantial $2\times$ range in ERF_{ari} sensitivity, from -0.0085 Wm^{-2} per Tg yr^{-1} (NorESM2) to -0.0191 Wm^{-2} per Tg yr^{-1} (CanAM5-PAM-Adj) (Fig. 2e). In contrast to ERF_{aci}, where it is better to compare the models' forcing versus iSSA number flux, for ERF_{ari} it is more meaningful to compare forcing per iSSA mass flux. This is because scattering of a single aerosol increases with the cross-sectional area of the particles $A \propto r^2$ while the mass scales with the volume $V \propto r^3$. The scattering per mass scales as $\propto \sigma_{scat} A/V$ for scattering efficiency σ_{scat} (Bellouin and Yu, 2022). For the aerosol size range we consider here (mainly in the accumulation mode), $\sigma_{scat} \propto r$, resulting in similar aerosol scattering per mass across the models despite different iSSA emission size distributions. This also means that the slope of ERF_{ari} vs. the iSSA number flux varies widely across the models (Fig. 2f).

CanAM5-PAM-Adj has particularly strong direct aerosol forcing, which we hypothesize is due to the ∼7 day iSSA lifetime in this model (Fig. 7), which is much longer than the ∼2.5 to 4.5 days in six of the other models (Fig. 7). We hypothesize that the long lifetime is due to strong precipitation suppression by the iSSA in the model, as the reduced precipitation rate in turn reduces the aerosol wet deposition rate and increases the residence time of aerosol in the troposphere. However, when we exclude CanAM5-PAM-Adj there is no longer a correlation between iSSA lifetime and direct aerosol forcing efficiency ($R^2 = 0.11$). Interestingly, we see that both CESM2-Ghosh and E3SMv2-Ghosh have a shorter iSSA lifetime and lower direct aerosol forcing efficiency than their default ARG2000 counterparts, CESM2 and E3SMv2. This may be due to the higher activation rates when using the Ghosh parameter changes to ARG2000, which increases the amount of cloud-borne aerosol and increases the rate of aerosol removal by precipitation formation.

6 Discussion and Conclusions

Improved ESM capabilities are crucial for credible assessments of the potential benefits, harms, and feasibility of solar radiation modification (SRM) technologies like MCB. This is particularly true for determining the potential climate impacts of SRM: because any test or experiment large enough to detectably alter the climate is indistinguishable from a deployment (Doherty et al., 2026), models are our only tool for estimating SRM's potential climate effects in advance of making deployment decisions. Notable recent progress has been made in our understanding of potential MCB climate effects (Haywood et al., 2023; Rasch et al., 2024; Chen et al., 2024a; Hirasawa et al., 2026a, b). However, inter-model differences in the representation of MCB radiative forcing remain large, making it difficult to use ESMs to credibly estimate the large-scale efficacy of MCB and thus estimate the iSSA emission rates that might be required for an actual deployment.

In this study, we aim to better quantify the range in MCB efficacy across different ESMs, with the aim of clarifying the processes driving inter-model spread and identifying paths toward better constraints. To do so, we compare the MCB ERF across six Coupled Model Intercomparison Project Phase 6 (CMIP6) models plus parameterization variants for three of those models. This represents the largest ESM inter-comparison for MCB using iSSA to date and provides an unprecedented quantification of non-linearity in the aerosol-cloud interactions by comparing the ESMs across a range of iSSA emission rates.

https://doi.org/10.5194/egusphere-2026-5460
Preprint. Discussion started: 21 September 2026

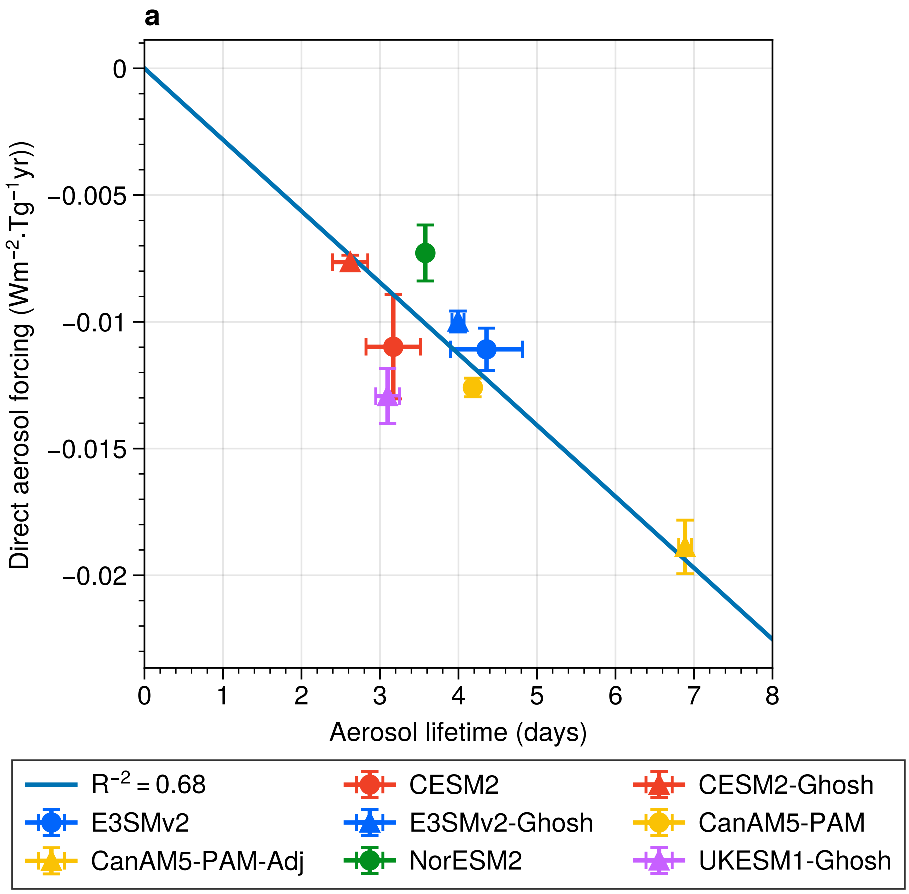

Figure 7. Direct aerosol forcing mass efficiency versus accumulation mode SSA lifetime for CESM2, CESM2-Ghosh, E3SMv2, E3SMv2-Ghosh, CanAM5-PAM, CanAM5-PAM-Adj, UKESM1-Ghosh, and NorESM2. x-error bars show one standard error in the linear regression used to compute the aerosol lifetime. y-error bars show the one standard error range of the direct aerosol forcing mass efficiency.

We find inter-ESM spread arises across the chain of processes from iSSA emission to cloud adjustments. The results here further emphasize the critical role of the emitted iSSA size distribution used in each model in determining MCB ERF_{aci} that have been previously highlighted in studies using parcel models (Connolly et al., 2014; Wood, 2021) and in previous ESM studies (Alterskjaer and Kristjánsson, 2013; Ahlm et al., 2017). In this study, different ESMs have adopted different iSSA size distributions that depended on the implementation of each model's natural wind-driven SSA emission parameterization and atmosphere aerosol size modes. This presents a challenge, because the model spread introduced by variations in the iSSA emission size distribution is large, but does not represent actual model structural uncertainty. Ideally, future intercomparisons would use aerosol treatments that ensure consistent iSSA size distributions across models. However, this may not be practical

https://doi.org/10.5194/egusphere-2026-5460
Preprint. Discussion started: 21 September 2026

in some models. Thus, careful documentation of emitted MCB iSSA size distributions and CCN diagnostics are necessary to properly interpret MCB signals.

Although aerosol activation is relatively well understood through κ-Köhler theory, differences in ESM parameterizations nevertheless drive large inter-model spread in activation rates, especially in polluted conditions. Like previous work (Alterskjaer and Kristjánsson, 2013; Connolly et al., 2014), we find that models using the Abdul-Razzak and Ghan (2000) activation parameterization (CESM2, E3SMv2, NorESM2, UKESM1) tend to saturate strongly at high CCN concentrations, and even have reductions in N_d at very high CCN concentrations. We examine the effect of the unrealistically strong vapour competition effect and consequent activation suppression in ARG2000 by conducting additional CESM2, E3SMv2, and UKESM1 simulations in which the ARG2000 parameterization is re-tuned to alleviate this artificially strong competition following Ghosh et al. (2025). Comparing CESM2-Ghosh, E3SMv2-Ghosh, and UKESM1-Ghosh to their default counterparts, we see that the new parameters significantly increase the activation rate, with saturation of activation occurring at much higher CCN concentrations, and we no longer see reductions in N_d at high emission rates. These changes result in much larger ERF_{aci} in these three models. We also examine the GFDL-AM4 model which has been noted to have ERF_{ari}-dominated MCB forcing (Mahfouz et al., 2023). We find this model produces very small cloud droplet activation fractions, likely because the activation parameterization uses a fixed size distribution and thus does not conserve iSSA number concentration. Other factors, such as the updrafts computed by the planetary boundary layer turbulence parameterization, background CCN, and the iSSA size distribution width also play important roles in inter-model differences in activation, which will be discussed in more detail in a forthcoming article.

Finally, we see large differences in ERF_{aci} from cloud adjustments, with one set of models showing weakly positive cloud fraction and LWP effects as N_d increases and another set of models showing strong increases in both. The importance of these effects is shown by comparing E3SMv2 versus CESM2 and CanAM5-PAM versus CanAM5-PAM-Adj. In E3SMv2, the KK2000 cloud droplet autoconversion scheme has been altered to better match in situ observations, substantially reducing its dependence on N_d compared to previous E3SM versions and CESM2, resulting in much weaker cloud adjustments (Ma et al., 2021). In CanAM5-PAM, the default configuration of the autoconversion parameterization assumes a constant N_d while the CanAM5-PAM-Adj configuration enables N_d dependence, resulting in strong cloud adjustments to iSSA. In both cases, this substantially increases the ERF_{aci} from MCB, with a factor of $\sim$2x difference between E3SMv2/CanAM5-PAM and CESM2/CanAM5-PAM-Adj. Interestingly, this 2x range due to cloud adjustments is smaller than the inter-model spread due to differences in iSSA size distribution and aerosol activation, indicating that MCB ERF_{aci} spread could be readily reduced by addressing these two relatively "low-hanging fruit" for which there is clearer process understanding. This is notable because cloud adjustments are the most difficult component of aerosol-cloud interaction chain to model and observationally constrain. Indeed, many ESMs do not include key sub-grid processes such as the entrainment response to cloud droplet sedimentation and sub-grid mesoscale circulations that influence the MCB cloud response (Feingold et al., 2024; Chun et al., 2023; McMichael et al., 2024).

In contrast to ERF_{aci}, the ERF_{ari} dependence on iSSA mass flux is relatively consistent across the ESMs at ≈ -0.1 Wm^{-2} per Tg yr^{-1} of iSSA. However, we do see some inter-model variations that are related to differences in aerosol lifetime. Because

https://doi.org/10.5194/egusphere-2026-5460
Preprint. Discussion started: 21 September 2026

ERF_{ari} increases consistently even at high iSSA emission rates, we see monotonic increases in MCB ERF_{tot} as iSSA emissions increase, even in cases where ERF_{aci} begins to decrease. Thus, these ESMs indicate that there is no regime where additional iSSA emissions will induce large-scale net warming, a concern that has been raised in previous work (Alterskjaer and Kristjánsson, 2013). However, it is the case that the efficiency of iSSA emissions decreases substantially as ERF_{aci} saturates.

Unlike previous studies (Ahlm et al., 2017; Mahfouz et al., 2024), we find that ERF_{aci} is the main source of forcing up to ~ -2 Wm^{-2} for seven of the ten models we tested here, and for nine of ten up to -1 Wm^{-2}. Indeed, GFDL-AM4 is the only model where ERF_{ari} is the dominant source of forcing for all emission rates we tested, which we attribute to its unrealistically weak iSSA activation rate (Mahfouz et al., 2024). We posit that the differences between this study and Ahlm et al. (2017) arise from: 1) smaller aerosol sizes used in this study, which results in much higher N_d concentrations (which drives ERF_{aci}) relative to SSA mass (which drives ERF_{ari}), 2) region selection, as we emit into the subtropical eastern Pacific and Atlantic stratocumulus regions only, in contrast to emitting into the entire tropics, 3) testing of lower emission rates, as ERF_{ari} tends to dominate at high emission rates when activation becomes saturated and even declines and because ERF_{ari} tends to mask the ERF_{aci} effect when free troposphere iSSA concentrations increase.

Furthermore, by computing the aerosol forcing across many different aerosol emission rates, we have been able to examine novel processes and interactions. We found that aerosol-cloud interactions can influence ERF_{ari} by modulating the aerosol lifetime, most notably in the case of CanAM5-PAM-Adj where N_d-induced precipitation suppression reduces iSSA wet deposition, thereby increasing ERF_{ari}. Conversely, we found that direct scattering by iSSA above clouds at higher emission rates can reduce the transmissivity of the free troposphere, thus reducing ERF_{aci}.

Based on these results, we posit that while the inter-ESM spread in MCB forcing is large, much of it can be readily resolved with modest model improvements. A critical first step would be to ensure consistent and realistic iSSA size distributions are used for MCB simulations. This may require that modelers introduce iSSA separately from the natural SSA parameterization. Since most modern models use two-moment modal aerosol schemes, emitting a number and mass flux corresponding to a consistent volume radius will substantially reduce model differences. Different choices in accumulation mode distribution width (e.g., geometric standard deviation, σ_g) will, however, still produce some model differences in emission size distribution. Secondly, activation parameterizations could be updated to treat accumulation mode iSSA particles separately from natural coarse mode SSA for models such as GFDL-AM4, or by re-tuning parameters in the commonly used ARG2000 to reduce the vapour competition effects at high CCN concentrations. The latter requires no structural changes to the models and substantially improves their performance for MCB conditions, slightly improves modeling of present-day N_d, and has modest effects on present-day climate (Ghosh et al., 2025; Riipinen et al., 2026). Furthermore, even without explicitly resolving these model differences, if models include key diagnostic variables, offline emulators can be used to reconcile the models if sufficiently detailed diagnostics are retained by modelers. In a follow-up study we will conduct such a comparison using a parcel model.

The results here indicate, however, that substantial inter-ESM differences will remain even after resolving differences in size distribution and activation parameterization. The representation of cloud adjustments in ESMs is a persistent challenge for evaluating the forcing from present-day anthropogenic and natural aerosol emission that will not be resolved without

https://doi.org/10.5194/egusphere-2026-5460
Preprint. Discussion started: 21 September 2026

deeper improvements to process understanding and process representation in ESMs. Thus, MCB studies will benefit from efforts to update aerosol and cloud parameterizations in ESMs using constraints from high resolution modeling, observations of experiments-of-opportunity, and potential future outdoor aerosol release studies. Conversely, modeling studies simulating MCB can provide insight into the representation of aerosol-cloud interactions because they conduct ESM simulations with large aerosol perturbations of well-known mass flux, number flux, and size distribution. As shown above, this enables clearer process comparisons across models than preindustrial to present-day aerosol emission changes, where it is necessary to account for secondary aerosol formation, differences in chemical processing, and the radiative effect of different aerosol species. These processes are likely not of primary importance in distinguishing model differences for MCB scenarios, and they require more detailed analysis of other non-linearities in aerosol-cloud interactions. More consistent treatment of the iSSA emissions with improving parameterizations together provides a path towards creating ESM simulations that can be credibly used to assess the feasibility, benefits, and harms of MCB as a potential future climate intervention.

Code and data availability. Analysis code and post-processed data to reproduce figures are available via Zenodo at Hirasawa (2026) (https://doi.org/10.5281/zenodo.22263021).

Author contributions. HH, KS, MH, JS, FB, and CW conducted simulations for this project. HH, PR, and KS designed the simulation protocol. HH analysed the data, generated figures, and prepared the original draft. All authors contributed to review and editing of the manuscript. SD, RW, and JH lead funding acquisition for this work.

Competing interests. The authors declare that they have no conflict of interest.

Acknowledgements. Support for Haruki Hirasawa, Knut von Salzen, Sarah Doherty, Rob Wood and Philip Rasch was provided by SilverLining's Safe Climate Research Initiative (SCRI) and through the University of Washington's Marine Cloud Brightening Research Program, which is funded by the generous support of a consortium of individual and foundation donors. Sarah Doherty's contribution to this publication is also partially funded by the Cooperative Institute for Climate, Ocean and Ecosystem Studies (CICOES) under NOAA Cooperative Agreement NA20OAR4320271, Contribution No. 2026-XXXX. Cindy Wang and Josh Smith acknowledge financial support by the Quadrature Climate Foundation. Support for Matthew Henry and James M. Haywood was provided by SilverLining's Safe Climate Research Initiative (SCRI). Cindy Wang and Josh Smith acknowledge financial support by the Quadrature Climate Foundation. James M. Haywood was also partially supported by Quadrature Climate Foundation. For Frida A.-M. Bender, computational resources were provided by the National Academic Infrastructure for Supercomputing in Sweden (NAISS), funded by the Swedish Research Council. Frida A.-M. Bender also acknowledges financial support from the Swedish e-Science Research Centre (SeRC), the Swedish Research Council Vetenskapsrådet (grant no. 2025-03620) and the Swedish Research Council for Sustainable Development Formas (grant no. 2025-02013)

https://doi.org/10.5194/egusphere-2026-5460
Preprint. Discussion started: 21 September 2026

References

Abdul-Razzak, H. and Ghan, S. J.: A parameterization of aerosol activation: 2. Multiple aerosol types, Journal of Geophysical Research: Atmospheres, 105, 6837–6844, https://doi.org/10.1029/1999JD901161, 2000.

Ackerman, A. S., Kirkpatrick, M. P., Stevens, D. E., and Toon, O. B.: The impact of humidity above stratiform clouds on indirect aerosol climate forcing, Nature, 432, 1014–1017, 2004.

Ahlm, L., Jones, A., Stjern, C. W., Muri, H., Kravitz, B., and Kristjánsson, J. E.: Marine cloud brightening – as effective without clouds, Atmospheric Chemistry and Physics, 17, 13 071–13 087, https://doi.org/10.5194/acp-17-13071-2017, 2017.

Albrecht, B. A.: Aerosols, Cloud Microphysics, and Fractional Cloudiness, Science, 245, 1227–1230, https://doi.org/10.1126/science.245.4923.1227, 1989.

Alterskjaer, K. and Kristjánsson, J. E.: The sign of the radiative forcing from marine cloud brightening depends on both particle size and injection amount: MARINE CLOUD BRIGHTENING, Geophysical Research Letters, 40, 210–215, https://doi.org/10.1029/2012GL054286, 2013.

Bellouin, N. and Yu, H.: Aerosol–radiation interactions, in: Aerosols and Climate, pp. 445–487, Elsevier, 2022.

Bellouin, N., Quaas, J., Gryspeerdt, E., Kinne, S., Stier, P., Watson-Parris, D., Boucher, O., Carslaw, K. S., Christensen, M., Daniau, A.-L., et al.: Bounding global aerosol radiative forcing of climate change, Reviews of Geophysics, 58, e2019RG000 660, 2020.

Bender, F.-M., Frey, L., McCoy, D. T., Grosvenor, D. P., and Mohrmann, J. K.: Assessment of aerosol–cloud–radiation correlations in satellite observations, climate models and reanalysis, Climate Dynamics, 52, 4371–4392, 2019.

Bretherton, C., Blossey, P. N., and Uchida, J.: Cloud droplet sedimentation, entrainment efficiency, and subtropical stratocumulus albedo, Geophysical research letters, 34, 2007.

Carslaw, K. S., Lee, L. A., Reddington, C. L., Pringle, K. J., Rap, A., Forster, P. M., Mann, G. W., Spracklen, D. V., Woodhouse, M. T., Regayre, L. A., and Pierce, J. R.: Large contribution of natural aerosols to uncertainty in indirect forcing, Nature, 503, 67–71, https://doi.org/10.1038/nature12674, 2013.

Chen, C.-C., Richter, J. H., Lee, W. R., MacMartin, D. G., and Kravitz, B.: Rethinking the susceptibility-based strategy for marine cloud brightening climate intervention: Experiment with CESM2 and its implications, Geophysical Research Letters, 51, e2024GL108 860, 2024a.

Chen, Y., Haywood, J., Wang, Y., Malavelle, F., Jordan, G., Partridge, D., Fieldsend, J., De Leeuw, J., Schmidt, A., Cho, N., Oreopoulos, L., Platnick, S., Grosvenor, D., Field, P., and Lohmann, U.: Machine learning reveals climate forcing from aerosols is dominated by increased cloud cover, Nature Geoscience, 15, 609–614, https://doi.org/10.1038/s41561-022-00991-6, 2022.

Chen, Y., Haywood, J., Wang, Y., Malavelle, F., Jordan, G., Peace, A., Partridge, D. G., Cho, N., Oreopoulos, L., Grosvenor, D., Field, P., Allan, R. P., and Lohmann, U.: Substantial cooling effect from aerosol-induced increase in tropical marine cloud cover, Nature Geoscience, 17, 404–410, https://doi.org/10.1038/s41561-024-01427-z, 2024b.

Chun, J.-Y., Wood, R., Blossey, P., and Doherty, S. J.: Microphysical, macrophysical, and radiative responses of subtropical marine clouds to aerosol injections, Atmospheric Chemistry and Physics, 23, 1345–1368, https://doi.org/10.5194/acp-23-1345-2023, 2023.

Coakley Jr, J. A. and Walsh, C. D.: Limits to the aerosol indirect radiative effect derived from observations of ship tracks, Journal of the Atmospheric Sciences, 59, 668–680, 2002.

Connolly, P. J., McFiggans, G. B., Wood, R., and Tsiamis, A.: Factors determining the most efficient spray distribution for marine cloud brightening, Philosophical Transactions of the Royal Society A: Mathematical, Physical and Engineering Sciences, 372, 20140 056, https://doi.org/10.1098/rsta.2014.0056, 2014.

Dana, M. T. and Hales, J. M.: Statistical aspects of the washout of polydisperse aerosols, Atmospheric Environment (1967), 10, 45–50, 1976.

Danabasoglu, G., Lamarque, J., Bacmeister, J., Bailey, D. A., DuVivier, A. K., Edwards, J., Emmons, L. K., Fasullo, J., Garcia, R., Gettelman, A., Hannay, C., Holland, M. M., Large, W. G., Lauritzen, P. H., Lawrence, D. M., Lenaerts, J. T. M., Lindsay, K., Lipscomb, W. H., Mills, M. J., Neale, R., Oleson, K. W., Otto-Bliesner, B., Phillips, A. S., Sacks, W., Tilmes, S., Van Kampenhout, L., Vertenstein, M., Bertini, A., Dennis, J., Deser, C., Fischer, C., Fox-Kemper, B., Kay, J. E., Kinnison, D., Kushner, P. J., Larson, V. E., Long, M. C., Mickelson, S., Moore, J. K., Nienhouse, E., Polvani, L., Rasch, P. J., and Strand, W. G.: The Community Earth System Model Version 2 (CESM2), Journal of Advances in Modeling Earth Systems, 12, e2019MS001 916, https://doi.org/10.1029/2019MS001916, 2020.

Derimian, Y., Dubovik, O., Huang, X., Lapyonok, T., Litvinov, P., Kostinski, A. B., Dubuisson, P., and Ducos, F.: Comprehensive tool for calculation of radiative fluxes: illustration of shortwave aerosol radiative effect sensitivities to the details in aerosol and underlying surface characteristics, Atmospheric Chemistry and Physics, 16, 5763–5780, 2016.

Diamond, M. S., Gettelman, A., Lebsock, M. D., McComiskey, A., Russell, L. M., Wood, R., and Feingold, G.: To assess marine cloud brightening's technical feasibility, we need to know what to study—and when to stop, Proceedings of the National Academy of Sciences, 119, e2118379 119, https://doi.org/10.1073/pnas.2118379119, 2022.

Doherty, S. J., Diamond, M. S., Wood, R., and Hirasawa, H.: Defining scales of field studies and experiments to assess marine cloud brightening, AGU Advances, 7, e2025AV001 939, 2026.

Feingold, G., Ghate, V. P., Russell, L. M., Blossey, P., Cantrell, W., Christensen, M. W., Diamond, M. S., Gettelman, A., Glassmeier, F., Gryspeerdt, E., Haywood, J., Hoffmann, F., Kaul, C. M., Lebsock, M., McComiskey, A. C., McCoy, D. T., Ming, Y., Mülmenstädt, J., Possner, A., Prabhakaran, P., Quinn, P. K., Schmidt, K. S., Shaw, R. A., Singer, C. E., Sorooshian, A., Toll, V., Wan, J. S., Wood, R., Yang, F., Zhang, J., and Zheng, X.: Physical science research needed to evaluate the viability and risks of marine cloud brightening, Science Advances, 10, eadi8594, https://doi.org/10.1126/sciadv.adi8594, 2024.

Gettelman, A. and Morrison, H.: Advanced Two-Moment Bulk Microphysics for Global Models. Part I: Off-Line Tests and Comparison with Other Schemes, Journal of Climate, 28, 1268–1287, https://doi.org/10.1175/JCLI-D-14-00102.1, 2015.

Ghan, S. J.: Technical Note: Estimating aerosol effects on cloud radiative forcing, Atmospheric Chemistry and Physics, 13, 9971–9974, https://doi.org/10.5194/acp-13-9971-2013, 2013.

Ghosh, P., Evans, K. J., Grosvenor, D. P., Kang, H.-G., Mahajan, S., Xu, M., Zhang, W., and Gordon, H.: Assessing modifications to the Abdul-Razzak and Ghan aerosol activation parameterization (version ARG2000) to improve simulated aerosol–cloud radiative effects in the UK Met Office Unified Model (UM version 13.0), Geoscientific Model Development, 18, 4899–4913, https://doi.org/10.5194/gmd-18-4899-2025, 2025.

Golaz, J., Van Roekel, L. P., Zheng, X., Roberts, A. F., Wolfe, J. D., Lin, W., Bradley, A. M., Tang, Q., Maltrud, M. E., Forsyth, R. M., Zhang, C., Zhou, T., Zhang, K., Zender, C. S., Wu, M., Wang, H., Turner, A. K., Singh, B., Richter, J. H., Qin, Y., Petersen, M. R., Mametjanov, A., Ma, P., Larson, V. E., Krishna, J., Keen, N. D., Jeffery, N., Hunke, E. C., Hannah, W. M., Guba, O., Griffin, B. M., Feng, Y., Engwirda, D., Di Vittorio, A. V., Dang, C., Conlon, L. M., Chen, C., Brunke, M. A., Bisht, G., Benedict, J. J., Asay-Davis, X. S., Zhang, Y., Zhang, M., Zeng, X., Xie, S., Wolfram, P. J., Vo, T., Veneziani, M., Tesfa, T. K., Sreepathi, S., Salinger, A. G., Reeves Eyre, J. E. J., Prather, M. J., Mahajan, S., Li, Q., Jones, P. W., Jacob, R. L., Huebler, G. W., Huang, X., Hillman, B. R., Harrop, B. E., Foucar, J. G., Fang, Y., Comeau, D. S., Caldwell, P. M., Bartoletti, T., Balaguru, K., Taylor, M. A., McCoy, R. B., Leung, L. R., and Bader, D. C.: The DOE

https://doi.org/10.5194/egusphere-2026-5460
Preprint. Discussion started: 21 September 2026

E3SM Model Version 2: Overview of the Physical Model and Initial Model Evaluation, Journal of Advances in Modeling Earth Systems, 14, e2022MS003 156, https://doi.org/10.1029/2022MS003156, 2022.

Gong, S.: A parameterization of sea-salt aerosol source function for sub-and super-micron particles, Global biogeochemical cycles, 17, 2003.

Gristey, J. J. and Feingold, G.: Stratospheric Aerosol Injection Would Change Cloud Brightness, Geophysical Research Letters, 52, e2024GL113 914, https://doi.org/10.1029/2024GL113914, 2025.

Haywood, J. M., Jones, A., Jones, A. C., and Rasch, P. J.: Climate Intervention using marine cloud brightening (MCB) compared with stratospheric aerosol injection (SAI) in the UKESM1 climate model, preprint, Aerosols/Atmospheric Modelling and Data Analysis/Troposphere/Physics (physical properties and processes), https://doi.org/10.5194/egusphere-2023-1611, 2023.

Hirasawa, H.: Data for: "On the Range of Marine Cloud Brightening Radiative Forcing across Earth System Models", https://doi.org/10.5281/zenodo.22263021, 2026.

Hirasawa, H., Henry, M., Mason, A. M., Rasch, P. J., Doherty, S. J., Wood, R., Haywood, J., and Von Salzen, K.: Forcing Susceptibility and Climate Sensitivity to Midlatitude Marine Cloud Brightening, Journal of Climate, 39, 769–784, 2026a.

Hirasawa, H., Henry, M., Rasch, P. J., Wood, R., Doherty, S. J., Haywood, J., Wong, A., Lamarque, J.-F., Brody, E., and Wang, H.: G6-1.5 K-MCB: Marine Cloud Brightening scenario design for the Geoengineering Model Intercomparison Project (GeoMIP) in CESM2. 1, E3SMv2. 0, and UKESM1. 1, Geoscientific Model Development, 19, 3257–3283, 2026b.

Holtslag, A., Svensson, G., Baas, P., Basu, S., Beare, B., Beljaars, A., Bosveld, F., Cuxart, J., Lindvall, J., Steeneveld, G., et al.: Stable atmospheric boundary layers and diurnal cycles: challenges for weather and climate models, Bulletin of the American Meteorological Society, 94, 1691–1706, 2013.

Jenkins, A., Forster, P., and Jackson, L.: The effects of timing and rate of marine cloud brightening aerosol injection on albedo changes during the diurnal cycle of marine stratocumulus clouds, Atmospheric Chemistry and Physics, 13, 1659–1673, 2013.

Jones, A., Haywood, J., and Boucher, O.: Climate impacts of geoengineering marine stratocumulus clouds, Journal of Geophysical Research: Atmospheres, 114, 2008JD011 450, https://doi.org/10.1029/2008JD011450, 2009.

Jones, A. C., Hill, A., Hemmings, J., Lemaitre, P., Quérel, A., Ryder, C. L., and Woodward, S.: Below-cloud scavenging of aerosol by rain: a review of numerical modelling approaches and sensitivity simulations with mineral dust in the Met Office's Unified Model, Atmospheric Chemistry and Physics, 22, 11 381–11 407, 2022.

Karset, I. H. H., Gettelman, A., Storelvmo, T., Alterskjær, K., and Berntsen, T. K.: Exploring impacts of size-dependent evaporation and entrainment in a global model, Journal of Geophysical Research: Atmospheres, 125, e2019JD031 817, 2020.

Khairoutdinov, M. and Kogan, Y.: A new cloud physics parameterization in a large-eddy simulation model of marine stratocumulus, Monthly weather review, 128, 229–243, 2000.

Kirkevåg, A., Grini, A., Olivié, D., Seland, Ø., Alterskjær, K., Hummel, M., Karset, I. H., Lewinschal, A., Liu, X., Makkonen, R., et al.: A production-tagged aerosol module for Earth system models, OsloAero5. 3–extensions and updates for CAM5. 3-Oslo, Geoscientific Model Development, 11, 3945–3982, 2018.

Kristiansen, N. I., Stohl, A., Oliviè, D. J. L., Croft, B., Søvde, O. A., Klein, H., Christoudias, T., Kunkel, D., Leadbetter, S. J., Lee, Y., et al.: Evaluation of observed and modelled aerosol lifetimes using radioactive tracers of opportunity and an ensemble of 19 global models, Atmospheric Chemistry and Physics, 16, 3525–3561, 2016.

Latham, J., Rasch, P., Chen, C.-C., Kettles, L., Gadian, A., Gettelman, A., Morrison, H., Bower, K., and Choularton, T.: Global temperature stabilization via controlled albedo enhancement of low-level maritime clouds, Philosophical Transactions of the Royal Society A: Mathematical, Physical and Engineering Sciences, 366, 3969–3987, https://doi.org/10.1098/rsta.2008.0137, 2008.

https://doi.org/10.5194/egusphere-2026-5460
Preprint. Discussion started: 21 September 2026

Liu, X., Ma, P.-L., Wang, H., Tilmes, S., Singh, B., Easter, R. C., Ghan, S. J., and Rasch, P. J.: Description and evaluation of a new four-mode version of the Modal Aerosol Module (MAM4) within version 5.3 of the Community Atmosphere Model, Geoscientific Model Development, 9, 505–522, https://doi.org/10.5194/gmd-9-505-2016, 2016.

Lohmann, U.: Anthropogenic aerosol influences on mixed-phase clouds, Current Climate Change Reports, 3, 32–44, 2017.

Ma, P.-L., Harrop, B. E., Larson, V. E., Neale, R., Gettelman, A., Morrison, H., Wang, H., Zhang, K., Klein, S. A., Zelinka, M. D., et al.: Better calibration of cloud parameterizations and subgrid effects increases the fidelity of E3SM Atmosphere Model version 1, Geoscientific Model Development Discussions, 2021, 1–57, 2021.

Ma, X., von Salzen, K., and Li, J.: Modelling sea salt aerosol and its direct and indirect effects on climate, Atmospheric Chemistry and Physics, 8, 1311–1327, 2008.

Mahfouz, N., Mülmenstädt, J., and Burrows, S.: Present-day correlations are insufficient to predict cloud albedo change by anthropogenic aerosols in E3SM v2, Atmospheric Chemistry and Physics, 24, 7253–7260, https://doi.org/10.5194/acp-24-7253-2024, 2024.

Mahfouz, N. G. A., Hill, S. A., Guo, H., and Ming, Y.: The Radiative and Cloud Responses to Sea Salt Aerosol Engineering in GFDL Models, Geophysical Research Letters, 50, e2022GL102 340, https://doi.org/10.1029/2022GL102340, 2023.

Mårtensson, E., Nilsson, E., de Leeuw, G., Cohen, L., and Hansson, H.-C.: Laboratory simulations and parameterization of the primary marine aerosol production, Journal of Geophysical Research: Atmospheres, 108, 2003.

McMichael, L. A., Schmidt, M. J., Wood, R., Blossey, P. N., and Patel, L.: Exploring ship track spreading rates with a physics-informed Langevin particle parameterization, Geoscientific Model Development, 17, 7867–7888, 2024.

Ming, Y., Ramaswamy, V., Donner, L. J., Phillips, V. T., Klein, S. A., Ginoux, P. A., and Horowitz, L. W.: Modeling the interactions between aerosols and liquid water clouds with a self-consistent cloud scheme in a general circulation model, Journal of the atmospheric sciences, 64, 1189–1209, 2007.

Monahan, E., Spiel, D., and Davidson, K.: A model of marine aerosol generation via whitecaps and wave disruption, in: Oceanic whitecaps: And their role in air-sea exchange processes, pp. 167–174, Springer, 1986.

Mulcahy, J. P., Johnson, C., Jones, C. G., Povey, A. C., Scott, C. E., Sellar, A., Turnock, S. T., Woodhouse, M. T., Abraham, N. L., Andrews, M. B., et al.: Description and evaluation of aerosol in UKESM1 and HadGEM3-GC3. 1 CMIP6 historical simulations, Geoscientific Model Development Discussions, 2020, 1–59, 2020.

Mulcahy, J. P., Jones, C. G., Rumbold, S. T., Kuhlbrodt, T., Dittus, A. J., Blockley, E. W., Yool, A., Walton, J., Hardacre, C., Andrews, T., et al.: UKESM1. 1: development and evaluation of an updated configuration of the UK Earth System Model, Geoscientific Model Development Discussions, 2022, 1–45, 2022.

Mülmenstädt, J., Ackerman, A. S., Fridlind, A. M., Huang, M., Ma, P.-L., Mahfouz, N., Bauer, S. E., Burrows, S. M., Christensen, M. W., Dipu, S., Gettelman, A., Leung, L. R., Tornow, F., Quaas, J., Varble, A. C., Wang, H., Zhang, K., and Zheng, Y.: Can general circulation models (GCMs) represent cloud liquid water path adjustments to aerosol–cloud interactions?, Atmospheric Chemistry and Physics, 24, 13 633–13 652, https://doi.org/10.5194/acp-24-13633-2024, 2024.

Nishant, N., Sherwood, S. C., and Geoffroy, O.: Aerosol-induced modification of organised convection and top-of-atmosphere radiation, npj Climate and Atmospheric Science, 2, 33, 2019.

Odoulami, R. C., Hirasawa, H., Kouadio, K., Patel, T. D., Quagraine, K. A., Pinto, I., Egbebiyi, T. S., Abiodun, B. J., Lennard, C., and New, M. G.: Africa's Climate Response to Marine Cloud Brightening Strategies Is Highly Sensitive to Deployment Region, Journal of Geophysical Research: Atmospheres, 129, e2024JD041 070, https://doi.org/10.1029/2024JD041070, 2024.

https://doi.org/10.5194/egusphere-2026-5460
Preprint. Discussion started: 21 September 2026

Petroff, A. and Zhang, L.: Development and validation of a size-resolved particle dry deposition scheme for application in aerosol transport models, Geoscientific Model Development, 3, 753–769, 2010.

Phinney, L. A., Lohmann, U., and Leaitch, W. R.: Limitations of using an equilibrium approximation in an aerosol activation parameterization, Journal of Geophysical Research: Atmospheres, 108, 2003.

Rasch, P. J., Latham, J., and Chen, C.-C. J.: Geoengineering by cloud seeding: influence on sea ice and climate system, Environmental Research Letters, 4, 045 112, https://doi.org/10.1088/1748-9326/4/4/045112, 2009.

Rasch, P. J., Hirasawa, H., Wu, M., Doherty, S. J., Wood, R., Wang, H., Jones, A., Haywood, J., and Singh, H.: A protocol for model intercomparison of impacts of marine cloud brightening climate intervention, Geoscientific Model Development, 17, 7963–7994, https://doi.org/10.5194/gmd-17-7963-2024, 2024.

Riipinen, I., Talvinen, S., Chassaing, A., Georgakaki, P., Li, X., García-Pando, C. P., Bergman, T., Kommula, S. M., Proske, U., Gkouvousis, A., et al.: Treatment of Key Aerosol and Cloud Processes in Earth System Models–Recommendations from the FORCeS Project: In honour of the memory of Prof. Astrid Kiendler-Scharr her contributions to atmospheric science, Tellus B: Chemical and Physical Meteorology, 78, 2026.

Rothenberg, D. and Wang, C.: Metamodeling of Droplet Activation for Global Climate Models, Journal of the Atmospheric Sciences, 73, 1255 – 1272, https://doi.org/10.1175/JAS-D-15-0223.1, 2016.

Rotstayn, L. D.: A physically based scheme for the treatment of stratiform clouds and precipitation in large-scale models. I: Description and evaluation of the microphysical processes, Quarterly Journal of the Royal Meteorological Society, 123, 1227–1282, 1997.

Salter, M. E., Zieger, P., Acosta Navarro, J. C., Grythe, H., Kirkevåg, A., Rosati, B., Riipinen, I., and Nilsson, E. D.: An empirically derived inorganic sea spray source function incorporating sea surface temperature, Atmospheric Chemistry and Physics, 15, 11 047–11 066, 2015.

Seland, Ø., Bentsen, M., Seland Graff, L., Olivié, D., Toniazzo, T., Gjermundsen, A., Debernard, J. B., Gupta, A. K., He, Y., Kirkevåg, A., et al.: The Norwegian Earth system model, NorESM2–evaluation of theCMIP6 DECK and historical simulations, Geoscientific Model Development Discussions, 2020, 1–68, 2020.

Sigmond, M., Anstey, J., Arora, V., Digby, R., Gillett, N., Kharin, V., Merryfield, W., Reader, C., Scinocca, J., Swart, N., et al.: Improvements in the Canadian Earth system model (CanESM) through systematic model analysis: CanESM5. 0 and CanESM5. 1, Geoscientific Model Development, 16, 6553–6591, 2023.

Stevens, B.: Rethinking the Lower Bound on Aerosol Radiative Forcing, Journal of Climate, 28, 4794–4819, https://doi.org/10.1175/JCLI-D-14-00656.1, 2015.

Varble, A. C., Igel, A. L., Morrison, H., Grabowski, W. W., and Lebo, Z. J.: Opinion: A critical evaluation of the evidence for aerosol invigoration of deep convection, Atmospheric Chemistry and Physics, 23, 13 791–13 808, 2023.

Vignesh, P. P., Jiang, J. H., Kishore, P., Su, H., Smay, T., Brighton, N., and Velicogna, I.: Assessment of CMIP6 cloud fraction and comparison with satellite observations, Earth and Space Science, 7, e2019EA000 975, 2020.

Virtanen, A., Joutsensaari, J., Kokkola, H., Partridge, D. G., Blichner, S., Seland, , Holopainen, E., Tovazzi, E., Lipponen, A., Mikkonen, S., Leskinen, A., Hyvärinen, A.-P., Zieger, P., Krejci, R., Ekman, A. M. L., Riipinen, I., Quaas, J., and Romakkaniemi, S.: High sensitivity of cloud formation to aerosol changes, Nature Geoscience, 18, 289–295, https://doi.org/10.1038/s41561-025-01662-y, 2025.

Von Salzen, K.: Piecewise log-normal approximation of size distributions for aerosol modelling, Atmospheric Chemistry and Physics, 6, 1351–1372, https://doi.org/10.5194/acp-6-1351-2006, 2006.

https://doi.org/10.5194/egusphere-2026-5460
Preprint. Discussion started: 21 September 2026

Von Salzen, K., Akingunola, A., Cole, J. N., Digby, R. A., Doherty, S. J., Fraser-Leach, L., Gryspeerdt, E., Sigmond, M., and Wood, R.: Reduced aerosol pollution diminished cloud reflectivity over the North Atlantic and Northeast Pacific, Nature Communications, 16, 9433, 2025.

Walters, D., Baran, A. J., Boutle, I., Brooks, M., Earnshaw, P., Edwards, J., Furtado, K., Hill, P., Lock, A., Manners, J., et al.: The Met Office Unified Model global atmosphere 7.0/7.1 and JULES global land 7.0 configurations, Geoscientific Model Development, 12, 1909–1963, 2019.

Wan, H., Yenpure, A., Geveci, B., Easter, R. C., Rasch, P. J., Zhang, K., and Zeng, X.: Features of mid-and high-latitude low-level clouds and their relation to strong aerosol effects in the Energy Exascale Earth System Model version 2 (E3SMv2), Geoscientific Model Development, 18, 5655–5680, 2025.

Wang, H., Peng, Y., von Salzen, K., Yang, Y., Zhou, W., and Zhao, D.: Evaluation of a Quasi-steady state approximation of the cloud Droplet Growth Equation (QDGE) scheme for aerosol activation in global models using multiple aircraft data over both continental and marine environments, Geoscientific Model Development Discussions, 2021, 1–30, 2021.

Wang, H., Peng, Y., von Salzen, K., Yang, Y., Zhou, W., and Zhao, D.: Evaluation of a quasi-steady-state approximation of the cloud droplet growth equation (QDGE) scheme for aerosol activation in global models using multiple aircraft data over both continental and marine environments, Geoscientific Model Development, 15, 2949–2971, 2022.

Wood, R.: Cancellation of aerosol indirect effects in marine stratocumulus through cloud thinning, Journal of the atmospheric sciences, 64, 2657–2669, 2007.

Wood, R.: Assessing the potential efficacy of marine cloud brightening for cooling Earth using a simple heuristic model, Atmospheric Chemistry and Physics, 21, 14 507–14 533, https://doi.org/10.5194/acp-21-14507-2021, 2021.

Wood, R., Field, P. R., and Cotton, W.: Autoconversion rate bias in stratiform boundary layer cloud parameterizations, Atmospheric Research, 65, 109–128, 2002.

Yuan, T., Song, H., Wood, R., Oreopoulos, L., Platnick, S., Wang, C., Yu, H., Meyer, K., and Wilcox, E.: Observational evidence of strong forcing from aerosol effect on low cloud coverage, Science Advances, 9, eadh7716, 2023.

Zelinka, M. D., Smith, C. J., Qin, Y., and Taylor, K. E.: Comparison of methods to estimate aerosol effective radiative forcings in climate models, Atmospheric Chemistry and Physics, 23, 8879–8898, https://doi.org/10.5194/acp-23-8879-2023, 2023.

Zhao, M., Golaz, J.-C., Held, I., Guo, H., Balaji, V., Benson, R., Chen, J.-H., Chen, X., Donner, L., Dunne, J., et al.: The GFDL global atmosphere and land model AM4. 0/LM4. 0: 1. Simulation characteristics with prescribed SSTs, Journal of Advances in Modeling Earth Systems, 10, 691–734, 2018.